Neutron-proton elastic scattering spin-spin correlation parameter measurements between 500 and 800 MeV. II. C_{SS} and C_{LS} at forward c.m. angles

T. Shima,* D. Hill, K. F. Johnson,† H. Shimizu,‡ H. Spinka, R. Stanek, D. Underwood, and A. Yokosawa
Argonne National Laboratory, Argonne, Illinois 60439

G. Glass, J. C. Hiebert, R. A. Kenefick, S. Nath,† and L. C. Northcliffe
Texas A&M University, College Station, Texas 77843

G. R. Burleson, R. W. Garnett,† J. A. Faucett,§ and M. W. Rawool-Sullivan§
New Mexico State University, Las Cruces, New Mexico 88003

R. Damjanovich and J. J. Jarmer
Los Alamos National Laboratory, Los Alamos, New Mexico 87545

R. H. Jeppesen
University of Montana, Missoula, Montana 59812

G. E. Tripard
Washington State University, Pullman, Washington 99164
(Received 18 June 1992)

Results are presented for the spin-spin correlation parameters C_{SS} and C_{LS} for free np elastic scattering at neutron beam kinetic energies of 484, 634, 720, and 788 MeV and c.m. angles between 25° and 80°. The measurements were performed with a polarized neutron beam and a polarized proton target. These are the first measurements of this type to be reported in the forward angular region with a free polarized neutron beam. The observables C_{SS} and C_{LS} are both small at all energies, except for C_{LS} at 788 MeV, which is larger than phase-shift analysis predictions by more than one standard deviation for most of the measured points.

PACS number(s): 13.75.Cs, 13.88.+e, 14.20.Pt, 21.30.+y

I. INTRODUCTION

A complete description of nucleon-nucleon (NN) elastic scattering requires knowledge of both isospin-1 ($I=1$) and isospin-0 ($I=0$) amplitudes as functions of angle and energy. The pp and nn elastic-scattering amplitudes are both pure $I=1$, whereas np and pn elastic-scattering amplitudes have an equal mixture of $I=1$ and 0. The five $I=0$ and five $I=1$ amplitudes [1] can be related to various spin asymmetries measured with polarized beams, polarized targets, and/or polarimeters to measure the outgoing nucleon spin [2,3]. The amplitudes can also be parametrized in terms of phase-shift and elasticity parameters [4]. Phase-shift analyses (PSA's) are commonly used to determine the amplitudes from fits to experimental data, with various theoretical inputs for the high partial waves and some of the elasticity parameters.

This experiment is one of a series of np experiments that have been performed at the Clinton P. Anderson Meson Physics Facility at Los Alamos (LAMPF) to aid in a determination of the $I=0$ amplitudes in the energy range between 500 and 800 MeV, where these amplitudes are poorly known. This is an extension of another experiment [5,6] using almost the same apparatus, in which pure C_{LL} and C_{SL} measurements were made for np elastic scattering in the c.m. angular range $80° < \theta_{\text{c.m.}} < 180°$. In yet another experiment [7], a number of mixed spin parameters $C'_{\alpha\beta}$ were measured. When all these measurements are combined, an angular distribution of the pure observables C_{LL}, $C_{SL}=C_{LS}$, and C_{SS} can be obtained for c.m. angles $25° < \theta_{\text{c.m.}} < 180°$ at incident neutron-beam kinetic energies of 484, 634, and 788 MeV. Measurements of other np elastic spin observables at these same energies are in progress [8] or have been performed. In addition, some spin observables have been obtained from quasielastic scattering of protons from deuterium. These will be discussed further in Sec. VII.

An important objective of this experiment is to study the energy dependence of spin asymmetries in np elastic

*Present address: Texas A&M University, College Station, TX 77843.
†Present address: AT Div., Los Alamos National Laboratory, Los Alamos, NM 87545.
‡Present address: Department of Physics, Yamagata University, Yamagata, Japan.
§Present address: MP Div., Los Alamos National Laboratory, Los Alamos, NM 87545.

scattering. These data will help in the search for structure that may exist in the $I=0$ channel. It has been shown in the past that there are several $I=1$ structures [9], which produce the resonancelike behavior in the $^1D_2$ and $^3F_3$ partial waves observed in the PSA's of Hoshizaki and co-workers [10,11], Arndt *et al.* [12], and the Saclay-Geneva group [13]. The structures were first seen [14] in a plot of $\Delta\sigma_L(I=1)$ and $k^2 C_{LL}\, d\sigma/d\Omega$, where $\Delta\sigma_L$ is the difference between the total cross sections for spin parallel and antiparallel states with longitudinally polarized beam and target. Since the $N\Delta$ and $d\pi$ channels cannot couple to $I=0$ by isospin conservation and since the masses of NN^*, N^*N^*, or $\Delta\Delta$ states are higher than the total energy available for an incident kinetic energy of 800 MeV, it is even more interesting to look for structures in the $I=0$ channel. Note that recent results [15] of $\Delta\sigma_L(I=0)$, extracted from the measurements of $\Delta\sigma_L(pp)$ and $\Delta\sigma_L(np)$, reveal structure near an incident kinetic energy of 634 MeV. Any structures in either the $I=1$ or 0 channel are of considerable interest because they may be evidence for dibaryons, which seem to be an unavoidable consequence inherent to the quark constituent model of nucleons [16].

This paper describes measurements of two spin-spin correlation parameters C_{LS} and C_{SS} in free np elastic scattering. The first subscript refers to the spin orientation of the beam and the second to that of the target,

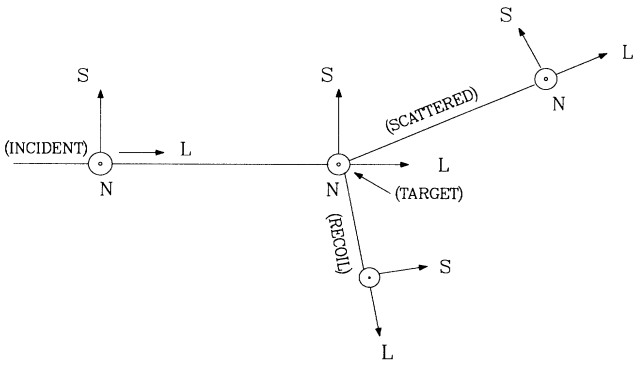

N: NORMAL TO THE SCATTERING PLANE
L: LONGITUDINAL DIRECTION
S= N x L IN THE SCATTERING PLANE

FIG. 1. Definitions of N-, S-, and L-type spins.

where $+L$ is along the beam direction, $+N$ is normal to the scattering plane, and $+S$ is in the scattering plane, as shown in Fig. 1. In the notation in which the differential cross section for beam spin in the $-i$ direction and target spin in the $+j$ direction is denoted $d\sigma/d\Omega(-+)$, etc., the spin parameters are defined by

$$C_{ij}=\frac{d\sigma/d\Omega(++)+d\sigma/d\Omega(--)-d\sigma/d\Omega(+-)-d\sigma/d\Omega(-+)}{d\sigma/d\Omega(++)+d\sigma/d\Omega(--)+d\sigma/d\Omega(+-)+d\sigma/d\Omega(-+)}\ . \tag{1}$$

The recoil protons were detected in a magnetic spectrometer, but the scattered neutrons could not be measured at the same time because of blocking by the polarized target magnet.

The polarized neutron beam, polarized proton target, and magnetic spectrometer are described in Secs. II, III, and IV, respectively. Details of the data analysis are presented in Sec. V. The results and the determination of the pure spin-spin correlation parameters are given in Sec. VI. Interpretation of the data and a comparison to phase-shift predictions are presented in Sec. VII. Reference [6] contains a detailed description of the physics motivation, experimental apparatus, and data analysis; only changes are described in detail in this paper.

II. POLARIZED NEUTRON BEAM

The beam and most of the experimental apparatus used for these measurements are the same as for a previous experiment [6]. Polarized protons were accelerated in the LAMPF linac to nominal kinetic energies of 497, 647, 733, and 800 MeV. After acceleration, the protons were transported in a well-shielded beam line to a liquid deuterium (LD_2) target, where the neutrons were produced at 0° in the reactions $\vec{p}+d\rightarrow\vec{n}+p+p$ and $\rightarrow\vec{n}+p+\pi+N$. The noninteracting primary protons and most of the other charged particles were deflected away from the 0° neutron path by bending magnets (LB-BM-06 and LB-BM-07; see Fig. 2). The neutron beam was collimated for a distance of 335 cm by a circular aperture of diameter 2.54 cm in a steel and lead channel through a thick concrete shielding wall. A lead plug of thickness 3.8 cm, positioned near the downstream end of the collimator, was used to absorb γ rays in the beam. The spectrum of the neutron-beam momentum consisted of a peak near the proton-beam momentum from the $\vec{p}d\rightarrow\vec{n}pp$ breakup reaction, which was enhanced by the pp final-state interaction. It was accompanied by a broad range of lower-momentum neutrons from other npp breakup processes and from pion production [17,18]. At proton energies of 497, 647, 733, and 800 MeV, the average neutron-beam kinetic energy in the peak is estimated to be 484, 634, 720, and 788 MeV, respectively. With 5–10 nA of proton beam, the intensity of the neutrons in the high-energy peak was a few thousand per second.

Production of neutrons at 0° was chosen to minimize the neutron peak width and to maximize the intensity. At this angle, however, the incident proton beam must be polarized in order for the neutrons to be polarized. Measurements [19,20] at three of the energies used in this experiment found relatively large spin-transfer parameters for longitudinally polarized protons and neutrons (K_{LL}),

but small values for transverse polarizations (K_{NN}). Hence proton beams with a large L-type spin component were used for the production of the polarized neutron beam.

The spin direction of the protons was reversed approximately every 2 min at the Lamb-shift polarized ion source. Aside from giving measurements of the cross sections in Eq. (1), this reversal helped to minimize systematic errors due to various slow changes in the experimental apparatus (efficiency, gain, timing, etc.). In the process of each spin reversal, there was a short period during which the polarized beam was "quenched" at the ion source, leaving primarily the background of unpolarized beam to be accelerated. The magnitude of the proton-beam polarization P_p (typically 80%) could be found from the ratio of beam intensities in the polarized and quenched periods [21].

The spin direction of the proton beam near the LD_2 target was continuously monitored by an in-line polarimeter [22]. The N and S components of the polarization at that point were measured directly. The L component was derived from these components and the value of P_p from the quench-beam information. After the polarimeter the beam was deflected magnetically through a horizontal angle of 16° before reaching the LD_2 target. During this deflection, the L and S components of the beam precessed somewhat in the horizontal plane. The orientation of the beam polarization at the LD_2 target was typically several degrees away from the L direction.

After the LD_2 target, the magnetic fields of LB-BM-06 and LB-BM-07 steered the proton beam to a beam dump. As a result, the direction of the neutron spin was precessed in the horizontal plane away from the L direction (45° at 484 MeV). In order to obtain the desired orientation of the beam polarization, the neutron-beam spin was corrected by the magnets LORRAINE and CASTOR, shown in Fig. 2. The excitation currents needed in these magnets to get either the L or S direction just before

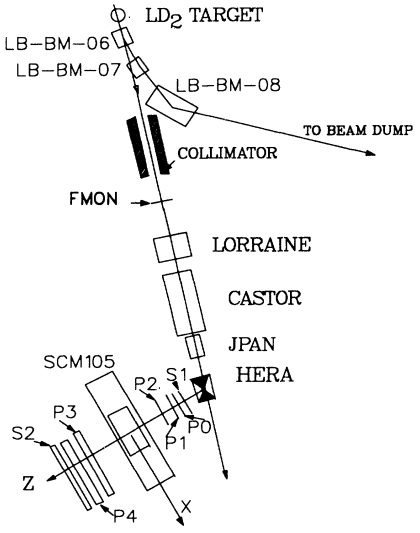

FIG. 2. Sketch of the experiment E770 layout (not to scale).

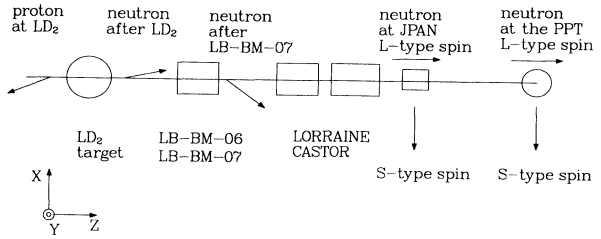

FIG. 3. Typical spin orientations at various places along the beam.

entering the field of the polarized target magnet (HERA) were determined empirically with a relative polarimeter JPAN, which was located downstream of CASTOR and measured the neutron polarization direction. JPAN was similar in design to an earlier neutron polarimeter [23], and is described in detail in Ref. [6]. JPAN was removed from the beam line after the desired LORRAINE and CASTOR currents had been established. Figure 3 illustrates a typical spin direction at each location from the LD_2 target to the polarized proton target. A study of the spin directions in this beam line has been made [24]. Small corrections [6] to these spin directions have been included for the results in this paper.

The polarization of the neutron beam for a proton polarization of P_p at an angle Ψ with respect to the beam may be expressed as

$$P_n=[(K_{LL}P_p\cos\Psi)^2+(K_{NN}P_p\sin\Psi)^2]^{1/2}\ , \qquad (2)$$

where K_{LL} and K_{NN} are the spin-transfer parameters for an L- and N-type proton beam, respectively. The values of K_{LL} were taken to be -0.499, -0.637, -0.620, and -0.604 at 484, 634, 720, and 788 MeV, respectively [20], from measurements made under very similar conditions to those of this experiment. The corresponding values of K_{NN} are -0.160, -0.079, -0.078, and -0.078. The estimated values of K_{LL} and K_{NN} may be modified in the future because of changes in the values of A_{np}, the np analyzing power, since they were obtained from asymmetry measurements which had to be divided by A_{np}.

Recent measurements of K_{LL} between 305 and 788 MeV made at LAMPF [8] differ by about 15% from those in Refs. [19] and [20]. However, the new data were taken under somewhat different beam conditions than those in this experiment or Ref. [20]. Work is in progress to understand the cause of the observed difference. It should be noted that for all data in this paper the renormalization would change the values by much less than one standard deviation. Thus there is relatively little impact on conclusions drawn from these data in comparison to phase-shift predictions, etc.

III. POLARIZED PROTON TARGET

The polarized proton target (PPT) setup consisted of a superconducting magnet (HERA), refrigerator, microwave source, and nuclear-magnetic-resonance (NMR) system [6,25–27]. Its operation was based on the

dynamic-nuclear-polarization (DNP) method [28] in which the target material is continually irradiated with microwaves. The superconducting coils of HERA were positioned to align the 2.5-T magnetic field in the horizontal plane, perpendicular to the beam direction, as shown in Fig. 3. Two different target materials, $C_3H_8O_2$ (propanediol) and a mixture of 85% by weight $C_2H_5(NH_2)$ (ethylamine) and 15% BH_3NH_3 (borane ammonia), were used during the experiment. Both were in the form of frozen beads doped with Cr^V to provide free electrons for microwave pumping. The latter material contained a factor of 1.6 higher fraction of polarizable free protons than the former, and it was used during the last half of the measurements reported here. The polarization of the PPT was reversed by a small change in the microwave frequency about every 8 h in order to provide the four different beam and target spin states $(++)$, $(+-)$, $(-+)$, and $(--)$; this also helped to reduce some systematic errors.

The polarization of the PPT was measured and monitored about every 2 min with the NMR system. Three NMR coils were placed at different locations surrounding the target material. One of the NMR coils was placed around the center and the other two toward each end of the target. The target material was contained in a flask which was 3.5 cm in diameter and 5.0 cm along the beam direction. The uniformity of the polarization over the target was checked with the three different coils and was found to differ by less than 1.8%. The calibration of the NMR system was accomplished by measurement of the polarization of the target material in thermal equilibrium (TE) at about 1 K, at which temperature the polarization is calculable. This calibration was performed 17 times in the 3 months during which these measurements were made. The total systematic error of the PPT system is estimated to be $\pm 3.3\%$, which comes mainly from a nonlinearity in the response of the NMR detectors. The typical PPT polarization was 75% during the experiment.

IV. SPECTROMETER AND DATA ACQUISITION

The magnetic spectrometer is shown schematically in Fig. 2. It consisted of a pair of scintillation counters $S1$, multiwire proportional chambers $P0$ and $P2$, drift chambers $P1$, $P3$, and $P4$, a large-aperture analyzing magnet designated SCM105, and a scintillation counter hodoscope $S2$. The spectrometer was identical to that described in Ref. [6], except that the chambers $P0$ and $P3$ were added to improve the momentum resolution and reconstruction efficiency. Chamber $P0$ was similar in construction to the $P2$ chambers, but its active area was 25.6×51.2 cm^2. Chamber $P3$ was identical to $P4$, and its readout scheme also used the delay-line technique [29]. Both $P0$ and $P2$ were mounted approximately perpendicular to the SCM105 center line, with $P0$ 230.8 cm upstream and $P3$ 135.0 cm downstream of the magnet center. Chamber $P0$ was centered on the SCM105 center line, and $P3$ was offset to the left by 52.9 cm. The spectrometer was centered at 57.5° to the incident neutron beam in the laboratory and was not moved during these measurements. Figure 4 shows some trajectories of the elastically scattered protons, viewed from above, along with the spectrometer. The SCM105 was operated at a reduced current of 1200 A, corresponding to $\int B\,dl \simeq 460$ kG cm, because the proton momenta were lower than in Ref. [6]. The center of this magnet was 331.5 cm from the polarized target.

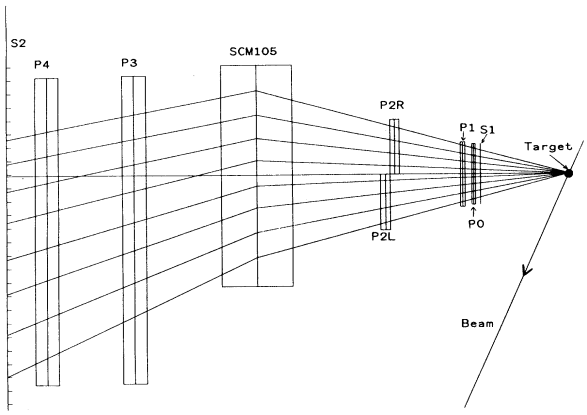

FIG. 4. Trajectories of particles through the spectrometer.

The event trigger was a coincidence of signals from both the $S1$ scintillation counters and any one of the $S2$ hodoscope counters. This trigger initiated the reading of the information from each chamber through CAMAC. In the case where $P2$ showed no hit, all chamber information was fast cleared to get ready for another trigger. Whenever the on-line computer was not busy with processing the events to tape, an on-line program then calculated the momentum by establishing the coordinates at each chamber. The efficiency of each chamber and rates in all the scintillators were also monitored, run by run, to check the performance of the apparatus.

V. OFF-LINE ANALYSIS OF DATA

The off-line analysis of the data was carried out in two phases. The first items to be established were the hodoscope and drift-chamber timing constants and spectrometer survey offsets. The spectrometer coordinate system is indicated in Fig. 2, with the origin located at the center of the spectrometer magnet. The survey offsets for $P1$, $P2$, and $P4$ were determined in the previous experiments [5,6]. Events taken with the SCM105 turned off were used to determine the alignment of $P0$ and $P3$. The offsets for $P0$ and $P3$ were chosen to minimize their deviations from straight-line fits to the other three chambers. The timing constants for the hodoscope counters and for $P1$, $P3$, and $P4$ were checked and calibrated as necessary, since significant timing drifts were occasionally encountered. After the calibrations were completed, data summary tapes (DSTs) were made from raw data tapes by an analysis program that removed the events lacking sufficient information for reconstruction of the trajectories of the scattered protons. This analysis program was identical to the one used previously [5–7] except for additional software needed to handle the data from $P0$

and $P3$ [30]. Typically 75% of the raw events were found reconstructable by the analysis program. The DST's contained only the position of the track at each chamber location for the reconstructable events, as well as the beam and target monitor information. Once the DST's were made, the necessary computer processing time for the off-line analysis was reduced by a factor of about 10, since there was no need for decoding of the wire information from the chambers.

In the second phase of the analysis, an accurate lookup table for $\int B\,dl$ in the spectrometer magnet was made, since the $\int B\,dl$ deviated significantly from its central value because of the large spectrometer aperture (84 cm high and 213 cm wide, corresponding to a solid angle ≈ 100 msr). The lookup tables at all energies were made with a computer program that generated elastic events with neutrons having known beam momenta which interacted in the polarized target. The energy loss due to the target material was not taken into account in this program, and only interactions from the center of the target were considered. The recoil protons were traced through the field of the polarized target magnet (PTM) and the SCM105. The computer program evaluated the $\int B\,dl$ from the resultant net bend in the trajectory. More than 2000 events were traced at each beam energy in order to establish the $\int B\,dl$ for the entire acceptance of the magnet.

The momentum for each DST event was determined from knowledge of the deflection angle and the $\int B\,dl$ map. The deflection angle was calculated from slopes before and after the spectrometer magnet, computed from the coordinates of each chamber. The scattering angles θ and ϕ were corrected for the modifications of the paths due to the S-type magnetic field of HERA. These corrections were given by analytic functions obtained from tracks through the PTM computed by a ray-tracing program.

When the DST events were plotted as a function of momentum and scattering angle (p and θ), the elastic locus over the region of acceptance was very nearly a straight line (see Fig. 5). A variable $\eta = p + A\theta + B$ could be defined which was orthogonal to this locus. The constants A and B were determined by the np elastic kinematics for protons at each energy. This choice for the variable, as opposed to the missing-mass variable used in Refs. [5–7], was prompted by the need to obtain a reliable estimate of the background. At the 57.5° setting of the spectrometer, the missing-mass histogram has an undesirable sharp cutoff above and close to the elastic peak region. Typical histograms of the variable η, used to extract the elastic signal, and the missing mass are shown in Figs. 6(a) and 6(b). The events in Figs. 6(a) and 6(b) have passed certain tests, such as having acceptable values of time of flight from $S1$ to $S2$, particle mass in the spectrometer, and projected target interaction point (interaction point in the X-Y plane of Fig. 2). Four separate histograms of η, corresponding to the four different initial spin states for the beam and target, were accumulated in 5° bins for c.m. angles between 22.5° and 82.5°.

The asymmetry for each 5°-angle bin was calculated

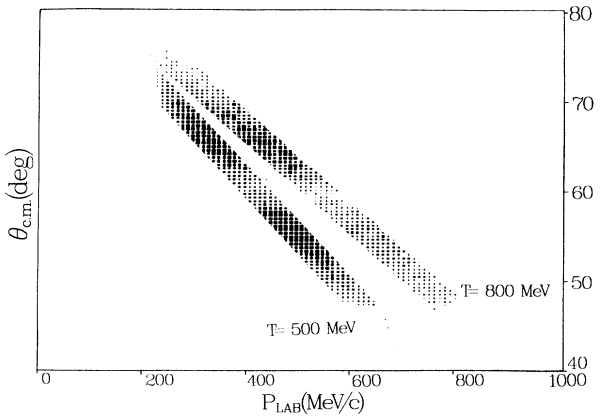

FIG. 5. Loci of np elastic kinematics in the angle-momentum plane, where the vertical and horizontal axes are the angle and momentum of protons, respectively. The bulk of the data have been eliminated to illustrate the central region corresponding to the kinematic loci for elastic np scattering at the two energies of 500 and 800 MeV. The lack of data near 60° c.m. results from the gap in the $P2$ chamber due to the chamber frames.

with the formula

$$\varepsilon = \frac{N(++)+N(--)-N(+-)-N(-+)}{N(++)+N(--)+N(+-)+N(-+)-N(\text{bkg})} \,. \tag{3}$$

In the equation above, $N(+-)$ is the yield for + beam spin and − target spin, etc., and N(bkg) is the background yield. These yields are all statistically independent and are functions of η. The N's correspond to the number of events passing cuts on particle mass and projected target interaction point from the spectrometer information, normalized to the integrated beam intensity. The relative beam intensity was measured with a set of scintillation counters (FMON) viewing a CH_2 target, located in the neutron beam between the collimator and LORRAINE. This same beam-intensity monitor was used previously and is described in detail in Ref. [6].

The background yield N(bkg) was based on data taken with carbon beads in the target flask in place of the polarizable material. The data corresponding to + and − beam spin were summed, since it was experimentally verified that there was no significant difference in the shapes of the η distributions. In principle, the background shapes might be very slightly different because of the expected polarization of ^{3}He or of the relatively small natural abundances of ^{13}C, ^{17}O, and ^{18}O nuclei in $C_3H_8O_2$. These effects in the $C_2H_5(NH_2)$ and BH_3NH_3 material could be significantly greater, because of the much larger amount of ^{14}N, ^{10}B, and ^{11}B that would be polarized. However, no evidence for differences in background shape was found for either the polarizable materials or carbon beads.

It was found that the carbon-bead background shape $N_C(\eta)$ did not completely match that for the polarized data for regions of η outside the elastic peak. The origin

of the difference in shapes is not known, but may be caused by (1) differences in η distributions of oxygen, nitrogen, and ^{3}He compared to carbon, (2) imperfect matching of the average carbon-bead and nonhydrogen densities in the polarizable material, or (3) multiple scattering of protons produced in pion production reactions off hydrogen. The ratio of the summed polarized data, $N_{\rm sum}=N(++)+N(--)+N(+-)+N(-+)$, to $N_C(\eta)$ was consistent with a straight line, $f(\eta)=G\eta+H$, within statistical errors, for η outside the elastic peak. Therefore N(bkg) in Eq. (3) was chosen to be $f(\eta)N_C$. This procedure was followed for each c.m.-angle bin and for each energy and spin observable. The η regions used to determine $f(\eta)$ changed very little as a function of beam energy.

The asymmetry ε was computed with Eq. (3) as a function of η in the elastic peak region. The weighted average of the individual asymmetries, $\varepsilon(\eta)$, in the elastic peak region was divided by the average neutron beam (P_n) and proton target (P_t) polarizations in order to obtain the mixed observables C'_{SS} and C'_{LS}:

$$C'_{\alpha\beta}=\frac{\langle\varepsilon\rangle}{P_nP_t}\ . \tag{4}$$

Tables I–IV list these observables and the associated statistical errors as a function of c.m. angle. The minimum and maximum limits to the c.m. angle are given for each bin, as well as the weighted average value derived from the data.

In order to check for internal consistency, a χ^2 per degree of freedom, $\chi^2/N_{\rm DF}$ was computed for each weighted asymmetry $\langle\varepsilon\rangle$. The values of $\chi^2/N_{\rm DF}$ ranged from 0.01 to 1.38, with typically 20 degrees of freedom, and are given in Tables I–IV. The largest average $\chi^2/N_{\rm DF}$ (1.38) occurred with the 634-MeV data, for which less carbon background data were taken because of problems associated with the $P3$ chamber at the beginning of the experiment.

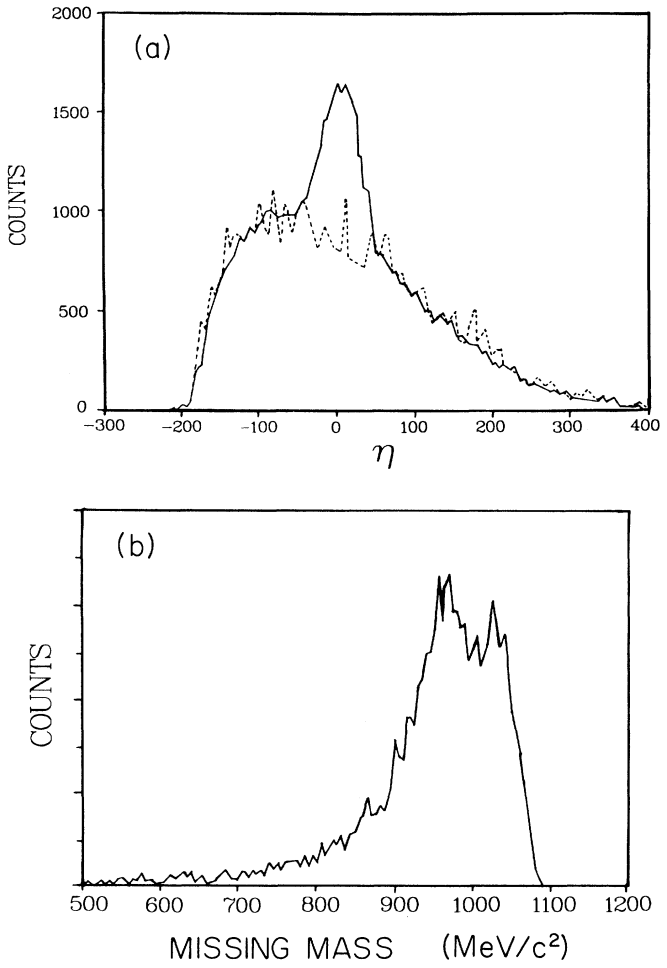

FIG. 6. Histograms showing the elastic signal. (a) The number of counts as a function of the variable η defined in the text at 484 MeV and $\theta_{\rm c.m.}=65°$. The dashed line gives the measured background counts normalized to the polarized target counts. (b) The missing-mass spectrum is shown at the same angle and energy.

VI. EXTRACTION OF THE PURE SPIN OBSERVABLES C_{SS} and C_{LS}

In the most general case, assuming parity conservation, the measured spin-spin correlation parameter $C'_{\alpha\beta}$ is a linear combination of the four pure parameters

$$C'_{\alpha\beta}=aC_{SS}+bC_{LL}+cC_{LS}+dC_{NN}\ . \tag{5}$$

The coefficient a is the product of the S components of the unit vectors for beam and target polarization, i.e., $(\vec{P}_n)_S(\vec{P}_t)_S/|\vec{P}_n||\vec{P}_t|$. The other coefficients b, c, and d are similarly related to the polarization components.

In this experiment there was negligible L component of the target polarization. Thus the coefficient b is zero. The other coefficients can be expressed in terms of three angles (see Fig. 7) as

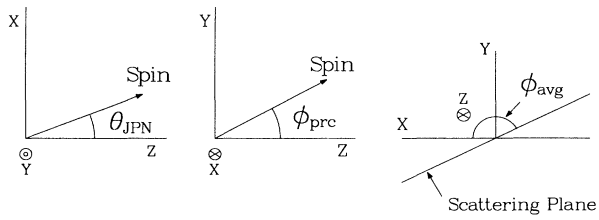

FIG. 7. Various angles needed in order to extract the pure spin observables using Eq. (6). All three angles $\theta_{\rm JPN}$, $\phi_{\rm prc}$, and $\phi_{\rm avg}$ along with their sign convention are shown in the figure.

TABLE I. Mixed spin observables at $T=484$ MeV. The quantities $\theta_{\min}$, $\theta_{\max}$, and $\langle\theta_{\text{c.m.}}\rangle$ are in degrees and represent the boundaries and central value of the c.m. angle for each bin, and the values of a, c, and d correspond to the coefficients in Eq. (5).

$\theta_{\min}$	$\theta_{\max}$	$\langle\theta_{\text{c.m.}}\rangle$	C'_{SS}	$\Delta C'_{SS}$	a	c	d	χ^2/N_{DF}
22.5	27.5	26.6	0.002	0.319	0.9614	−0.0922	0.0338	0.50
27.5	32.5	30.6	0.136	0.512	0.9749	−0.0929	0.0203	0.11
32.5	37.5	35.2	0.017	0.182	0.9795	−0.0931	0.0157	0.74
37.5	42.5	40.1	0.078	0.084	0.9778	−0.0930	0.0175	0.53
42.5	47.5	45.0	0.133	0.071	0.9768	−0.0930	0.0184	0.89
47.5	52.5	49.8	0.184	0.067	0.9782	−0.0930	0.0170	0.51
52.5	57.5	55.2	0.049	0.081	0.9513	−0.0917	0.0439	0.83
57.5	62.5	60.3	0.148	0.061	0.9534	−0.0918	0.0418	0.36
62.5	67.5	65.0	0.045	0.058	0.9582	−0.0920	0.0371	0.42
67.5	72.5	69.9	0.020	0.074	0.9582	−0.0920	0.0371	0.96
72.5	77.5	74.7	−0.049	0.100	0.9639	−0.0923	0.0313	0.72
77.5	82.5	78.9	0.104	0.202	0.9749	−0.0929	0.0203	1.14
22.5	27.5	26.6	0.143	0.417	−0.0400	0.9445	0.0523	0.26
27.5	32.5	30.6	−0.325	0.294	−0.0294	0.9517	0.0416	0.44
32.5	37.5	35.2	−0.059	0.213	−0.0248	0.9542	0.0371	0.75
37.5	42.5	40.1	−0.047	0.085	−0.0267	0.9532	0.0389	0.38
42.5	47.5	45.0	0.078	0.065	−0.0276	0.9527	0.0398	0.57
47.5	52.5	49.8	−0.074	0.068	−0.0262	0.9535	0.0384	0.89
52.5	57.5	55.2	0.002	0.077	−0.0456	0.9392	0.0588	0.94
57.5	62.5	60.3	0.064	0.059	−0.0453	0.9404	0.0575	0.59
62.5	67.5	64.5	−0.041	0.056	−0.0422	0.9429	0.0544	1.03
67.5	72.5	69.9	−0.010	0.071	−0.0422	0.9429	0.0544	0.88
72.5	77.5	74.7	0.027	0.100	−0.0383	0.9459	0.0505	0.75
77.5	82.5	78.9	−0.016	0.184	−0.0294	0.9517	0.0416	0.69

$$C'_{\alpha\beta}=C_{SS}(\sin\theta_{\text{JPN}}\cos^2\phi_{\text{avg}}-\sin\phi_{\text{prc}}\cos\theta_{\text{JPN}}\sin\phi_{\text{avg}}\cos\phi_{\text{avg}})+C_{LS}(\cos\phi_{\text{prc}}\cos\theta_{\text{JPN}}\cos\phi_{\text{avg}})$$
$$+C_{NN}(\sin\theta_{\text{JPN}}\sin^2\phi_{\text{avg}}+\sin\phi_{\text{prc}}\cos\theta_{\text{JPN}}\sin\phi_{\text{avg}}\cos\phi_{\text{avg}})\ . \tag{6}$$

The neutron-beam spin, before entrance into the magnetic field of the PPT, contained a negligible N component. In the equation above, θ_{JPN} is the angle between the beam polarization and longitudinal ($+L$) direction before the PPT. The field at the PPT did not affect the S component of the beam spin. However, the polarized target magnet introduced a precession by an angle ϕ_{prc} of the L component of the neutron spin in passage to the center of the target. Finally, the average scattering plane was slightly rotated from the horizontal ($\phi_{\text{avg}}=180°$) because of the effect of the spectrometer acceptance and the target magnetic field on the recoil proton trajectories.

Typical values for these angles are $\phi_{\text{prc}}\simeq 15°$, $\phi_{\text{avg}}\simeq 170°$, and $\theta_{\text{JPN}}\simeq 3°$ and 80° for L- and S-type neutron beams, respectively. The rotation ϕ_{avg} of the scattering plane was determined from the detected events and is a function of the scattering angle. The coefficients a, c, and d for the measured parameters C'_{SS} and C'_{LS} were computed from Eq. (6) with use of the known beam-spin direction (see Sec. II), the measured field map for HERA, and ϕ_{avg}. These coefficients are given in Tables I–IV along with the values of C'_{SS} and C'_{LS} for 484, 634, 720, and 788 MeV, respectively.

In order to derive pure C_{SS} and C_{LS} values, the values for C_{NN} are taken from the phase-shift analysis of Arndt *et al.* [31]. The contribution dC_{NN} to $C'_{\alpha\beta}$ in Eq. (5) is small with respect to the other terms, since the coefficient d is small. The equations for C'_{SS} and C'_{LS} can then be solved for the pure spin-spin correlation parameters. The results are given in Table V. The data at 634 and 788 MeV are divided into four or five independent sets of runs corresponding to different beam-spin conditions and dates in Tables II and IV. The χ^2 values at each angle are also given in Table V for these two energies. Note that the values of C_{SS} and C_{LS} differ from C'_{SS} and C'_{LS}, respectively, by typically no more than 0.03.

VII. RESULTS AND DISCUSSION

The values of C_{SS} and C_{LS}, along with the existing data [6,7,32], are plotted in Figs. 8(a)–8(h). The PSA predictions of Arndt *et al.* [12,31], Hashimoto, Higuchi, and Hoshizaki [33], and Bugg [34] are displayed by chain-dashed, chain-dotted, and dashed lines, respectively. The χ^2 values for the PSA predictions of Arndt, Bugg, Bystricky, Lechanoine-Lelue, and Lehar [13], the newer PSA results of Hoshizaki and co-workers [11], and the model predictions of Lee and co-workers [35] for C_{SS}

and C_{LS} are given in Table VI. The quality of all recent predictions are similar, and thus not all these predictions are given in Figs. 8(a)–8(h). Note that the quantity AZX calculated in the SAID computer program [31] is $-C_{LS}=-C_{SL}$ using the definition of these spin observables in this paper.

The values of C_{SS} at the forward-scattering angles (25°–80°) agree with all the predictions at the lower energies, but differ significantly with all but Bugg's result [34] at 788 MeV. All the predictions for C_{LS}, except at 788 MeV, also are consistent with these measurements. Each value of C_{LS} at 788 MeV was obtained by two independent sets of data taken about 2 months apart. Therefore the disagreement on the C_{LS} values with the PSA predictions at 788 MeV is less likely to be due to a normalization error in either the measured target polarization or in the integrated beam intensity. These values of $\chi^2/N_{\rm DF}$ of the data from the five sets of runs were less than 1.0 except at a c.m. angle of 78.1°, which is at the edge of the spectrometer acceptance, and where $\chi^2/N_{\rm DF}$ was 2.39

TABLE II. Mixed spin observables at $T=634$ MeV. The symbols are the same as in Table I.

$\theta_{\rm min}$	$\theta_{\rm max}$	$\langle\theta_{\rm c.m.}\rangle$	C'_{SS}	$\Delta C'_{SS}$	a	c	d	$\chi^2/N_{\rm DF}$
22.5	27.5	25.8	−0.613	1.775	0.9539	−0.0779	0.0428	0.22
27.5	32.5	30.7	−0.025	0.470	0.9709	−0.0786	0.0258	1.05
32.5	37.5	35.4	−0.015	0.118	0.9746	−0.0788	0.0220	1.09
37.5	42.5	40.1	0.037	0.192	0.9756	−0.0788	0.0210	0.62
42.5	47.5	45.0	−0.103	0.114	0.9766	−0.0789	0.0200	1.09
47.5	52.5	49.6	0.151	0.119	0.9799	−0.0790	0.0167	0.77
52.5	57.5	55.3	−0.439	0.194	0.9473	−0.0776	0.0493	0.40
57.5	62.5	60.1	−0.034	0.095	0.9503	−0.0778	0.0464	1.13
62.5	67.5	64.9	0.015	0.148	0.9488	−0.0777	0.0478	0.87
67.5	72.5	69.8	0.149	0.141	0.9525	−0.0779	0.0442	0.95
72.5	77.5	74.4	0.102	0.165	0.9619	−0.0783	0.0347	0.64
77.5	82.5	78.4	−1.282	1.084	0.9741	−0.0788	0.0225	0.18
22.5	27.5	25.8	−0.250	1.665	0.9552	−0.0813	0.0412	0.94
27.5	32.5	30.7	0.075	0.421	0.9718	−0.0820	0.0245	0.28
32.5	37.5	35.4	−0.068	0.174	0.9764	−0.0822	0.0199	0.48
37.5	42.5	40.1	0.194	0.123	0.9774	−0.0823	0.0189	0.74
42.5	47.5	45.0	0.188	0.096	0.9769	−0.0823	0.0194	0.30
47.5	52.5	49.6	0.165	0.128	0.9750	−0.0822	0.0214	0.80
52.5	57.5	55.3	0.288	0.205	0.9441	−0.0808	0.0522	0.32
57.5	62.5	60.1	0.226	0.076	0.9565	−0.0813	0.0398	0.64
62.5	67.5	64.9	0.107	0.099	0.9592	−0.0815	0.0371	0.76
67.5	72.5	69.8	0.288	0.111	0.9612	−0.0816	0.0352	0.41
72.5	77.5	74.4	0.184	0.145	0.9679	−0.0819	0.0284	0.54
77.5	82.5	78.4	−0.203	0.308	0.9783	−0.0823	0.0180	0.84
22.5	27.5	25.8	0.878	0.808	−0.1929	0.9401	0.0399	0.16
27.5	32.5	30.7	−0.385	0.400	−0.1861	0.9485	0.0331	0.70
32.5	37.5	35.4	−0.078	0.742	−0.1838	0.9507	0.0309	0.24
37.5	42.5	40.1	−0.194	0.122	−0.1833	0.9512	0.0303	0.50
42.5	47.5	45.0	−0.029	0.094	−0.1824	0.9519	0.0294	0.89
47.5	52.5	49.6	0.083	0.109	−0.1806	0.9534	0.0276	1.38
52.5	57.5	55.3	0.061	0.239	−0.1950	0.9367	0.0420	1.03
57.5	62.5	60.1	−0.115	0.087	−0.1941	0.9382	0.0411	0.52
62.5	67.5	64.9	−0.156	0.129	−0.1948	0.9371	0.0418	1.02
67.5	72.5	69.8	−0.052	0.143	−0.1934	0.9393	0.0404	1.36
72.5	77.5	74.4	−0.124	0.173	−0.1901	0.9439	0.0372	0.84
77.5	82.5	78.4	−0.936	0.541	−0.1847	0.9499	0.0317	0.87
22.5	27.5	25.8	0.492	1.312	−0.1894	0.9409	0.0399	0.01
27.5	32.5	30.7	0.328	0.425	−0.1822	0.9495	0.0327	0.45
32.5	37.5	35.4	0.262	0.138	−0.1796	0.9519	0.0301	0.44
37.5	42.5	40.1	0.091	0.122	−0.1790	0.9524	0.0295	1.30
42.5	47.5	45.0	−0.024	0.105	−0.1793	0.9522	0.0298	0.69
47.5	52.5	49.6	−0.093	0.127	−0.1805	0.9512	0.0310	0.54
52.5	57.5	55.3	−0.062	0.172	−0.1929	0.9352	0.0434	0.58
57.5	62.5	60.1	−0.091	0.076	−0.1889	0.9416	0.0394	1.29
62.5	67.5	64.9	0.056	0.101	−0.1879	0.9430	0.0384	1.17
67.5	72.5	69.8	0.050	0.108	−0.1871	0.9440	0.0376	0.46
72.5	77.5	74.4	0.177	0.143	−0.1842	0.9475	0.0346	0.79
77.5	82.5	78.4	−0.057	0.326	−0.1784	0.9529	0.0289	0.23

TABLE III. Mixed spin observables at $T=720$ MeV. The symbols are the same as in Table I.

$\theta_{\min}$	$\theta_{\max}$	$\langle\theta_{\text{c.m.}}\rangle$	C'_{SS}	$\Delta C'_{SS}$	a	c	d	χ^2/N_{DF}
22.5	27.5	25.7	0.403	0.569	0.9578	0.0084	0.0422	0.98
27.5	32.5	30.6	−0.089	0.226	0.9719	0.0084	0.0281	0.33
32.5	37.5	35.1	0.210	0.234	0.9757	0.0084	0.0242	0.75
37.5	42.5	40.1	−0.112	0.181	0.9773	0.0084	0.0226	0.52
42.5	47.5	45.0	0.162	0.150	0.9789	0.0084	0.0211	0.64
47.5	52.5	49.8	−0.046	0.193	0.9752	0.0084	0.0248	0.57
52.5	57.5	55.4	0.356	0.201	0.9426	0.0083	0.0573	1.05
57.5	62.5	60.1	0.326	0.119	0.9571	0.0083	0.0429	0.44
62.5	67.5	64.9	0.203	0.152	0.9585	0.0084	0.0415	1.28
67.5	72.5	69.8	0.217	0.202	0.9619	0.0084	0.0381	0.88
72.5	77.5	74.3	0.340	0.343	0.9701	0.0084	0.0299	0.24
77.5	82.5	78.3	−1.937	1.472	0.9818	0.0085	0.0182	0.41
22.5	27.5	25.7	0.030	0.525	−0.1037	0.9551	0.0392	1.24
27.5	32.5	30.6	0.023	0.492	−0.0971	0.9621	0.0326	0.33
32.5	37.5	35.1	0.198	0.492	−0.0971	0.9621	0.0326	0.33
37.5	42.5	40.1	−0.116	0.118	−0.0940	0.9648	0.0295	0.75
42.5	47.5	45.0	−0.013	0.167	−0.0931	0.9655	0.0285	0.60
47.5	52.5	49.8	0.363	0.192	−0.0953	0.9637	0.0307	0.56
52.5	57.5	55.4	0.068	0.238	−0.1093	0.9476	0.0448	0.67
57.5	62.5	60.1	−0.007	0.135	−0.1040	0.9548	0.0395	0.51
62.5	67.5	64.9	0.028	0.160	−0.1034	0.9555	0.0389	0.46
67.5	72.5	69.8	−0.029	0.238	−0.1020	0.9572	0.0374	0.46
72.5	77.5	74.3	0.025	0.282	−0.0981	0.9612	0.0335	0.46
77.5	82.5	78.3	0.279	0.916	−0.0911	0.9669	0.0266	0.66

(see Table V).

One interesting feature of the observable C_{SS} appears when the 634-MeV results are compared with those for 788 MeV. At 634 MeV, C_{SS} shows a prominent peak and dip in an angular region between 25° and 120° as seen in Fig. 8(b), while C_{SS} at 788 MeV seems to be flat in this angular region. A dip and peak also appear [5,6] in C_{LL} between 90° and 125° at 634 MeV. Recently, a structure in $\Delta\sigma_L(I=0)$ was reported [15] which has a peak around 634 MeV. It is uncertain at this time whether or not the peak and/or dip in C_{SS} might be related to the structure in $\Delta\sigma_L(I=0)$. It is also somewhat surprising that the average value for C_{LS} at 788 MeV in the forward-scattering region (25°–80° in disagreement with PSA predictions) rises up to 0.263 ± 0.039, while it is consistent with zero at lower energies (in agreement with the PSA predictions). Note that the observable C_{LS} must vanish at 0° and 180°. It is also expected to become small as the c.m. energy increases if nucleon helicity is conserved.

The solid lines in Fig. 8 represent least-squares fits to all the data with a ninth-order polynomial in $\cos\theta$. The highest-order polynomial needed to fit the data was estimated by a method based on the F distribution expressed as a function of χ^2 [36].

To investigate the behavior of the spin observables further, it is convenient to define the amplitudes

$$\phi_s=(\phi_1-\phi_2)/2=(\langle++|++\rangle-\langle++|--\rangle)/2\ ,$$
$$\phi_t=(\phi_1+\phi_2)/2=(\langle++|++\rangle+\langle++|--\rangle)/2\ ,$$
$$\phi_T=(\phi_3-\phi_4)/2=(\langle+-|+-\rangle-\langle+-|-+\rangle)/2\ ,$$
$$\phi_\tau=(\phi_3+\phi_4)/2=(\langle+-|+-\rangle+\langle+-|-+\rangle)/2\ ,$$
$$\phi_5=\phi_5=\langle++|+-\rangle\ ,$$

where ϕ_1, ϕ_2, ϕ_3, ϕ_4, and ϕ_5 are the usual helicity amplitudes as defined in Ref. [1] (in the equations above, the + and − refer to the nucleon helicities). The amplitude ϕ_s contains only spin-singlet contributions, ϕ_T and ϕ_τ contain only spin-triplet partial waves, and ϕ_t and ϕ_5 contain only coupled spin-triplet terms [1]. Some observables of interest in terms of these amplitudes are [37]

$$\frac{d\sigma}{d\Omega}=|\phi_{s,I}|^2+|\phi_{t,I}|^2+|\phi_{T,I}|^2+|\phi_{\tau,I}|^2+2|\phi_{5,I}|^2\ , \tag{7}$$

$$P\frac{d\sigma}{d\Omega}=2\,\mathrm{Im}(\phi^*_{t,I}\phi_{5,I}-\phi_{T,I}\phi^*_{5,I})\ , \tag{8}$$

$$C_{LS}\frac{d\sigma}{d\Omega}=2\,\mathrm{Re}(\phi^*_{t,I}\phi_{5,I}-\phi_{T,I}\phi^*_{5,I})\ , \tag{9}$$

$$C_{SS}\frac{d\sigma}{d\Omega}=-|\phi_{s,I}|^2+|\phi_{t,I}|^2-|\phi_{T,I}|^2+|\phi_{\tau,I}|^2\ , \tag{10}$$

$$C_{LL}\frac{d\sigma}{d\Omega}=-|\phi_{s,I}|^2-|\phi_{t,I}|^2+|\phi_{T,I}|^2+|\phi_{\tau,I}|^2\ , \tag{11}$$

$$C_{NN}\frac{d\sigma}{d\Omega}=-|\phi_{s,I}|^2+|\phi_{t,I}|^2+|\phi_{T,I}|^2-|\phi_{\tau,I}|^2+2|\phi_{5,I}|^2\ , \tag{12}$$

where these expressions hold for both $I=0$ and 1. The pure $I=0$ spin observables are given by [37]

TABLE IV. Mixed spin observables at $T=788$ MeV. The symbols are the same as in Table I.

$\theta_{\min}$	$\theta_{\max}$	$\langle\theta_{\text{c.m.}}\rangle$	C'_{SS}	$\Delta C'_{SS}$	a	c	d	χ^2/N_{DF}
22.5	27.5	25.8	−0.047	0.467	0.9568	−0.1036	0.0373	0.96
27.5	32.5	30.6	−0.022	0.441	0.9711	−0.1044	0.0231	0.30
32.5	37.5	35.4	−0.253	0.395	0.9741	−0.1046	0.0200	0.42
37.5	42.5	40.1	0.052	0.317	0.9756	−0.1047	0.0186	0.38
42.5	47.5	44.9	0.239	0.201	0.9760	−0.1047	0.0181	0.60
47.5	52.5	49.8	0.158	0.226	0.9721	−0.1045	0.0220	0.52
52.5	57.5	55.4	0.026	0.164	0.9441	−0.1029	0.0501	0.50
57.5	62.5	60.0	−0.109	0.130	0.9542	−0.1035	0.0400	0.71
62.5	67.5	64.9	0.158	0.162	0.9521	−0.1034	0.0421	0.90
67.5	72.5	69.8	0.422	0.531	0.9548	−0.1035	0.0393	0.20
72.5	77.5	74.1	−0.088	0.445	0.9655	−0.1041	0.0286	0.37
77.5	82.5	78.1	0.057	0.358	0.9774	−0.1048	0.0168	0.40
22.5	27.5	25.8	0.213	0.798	0.9553	0.0452	0.0436	0.26
27.5	32.5	30.6	−0.196	0.263	0.9707	0.0456	0.0281	0.17
32.5	37.5	35.4	0.148	0.147	0.9741	0.0456	0.0248	0.46
37.5	42.5	40.1	−0.152	0.100	0.9757	0.0457	0.0232	0.70
42.5	47.5	44.9	0.010	0.086	0.9762	0.0457	0.0227	0.72
47.5	52.5	49.8	0.183	0.124	0.9719	0.0456	0.0270	0.42
52.5	57.5	55.4	−0.018	0.110	0.9415	0.0449	0.0574	0.66
57.5	62.5	60.0	0.046	0.086	0.9524	0.0451	0.0465	0.73
62.5	67.5	64.9	0.138	0.121	0.9501	0.0451	0.0488	0.53
67.5	72.5	69.8	0.229	0.205	0.9531	0.0452	0.0458	0.72
72.5	77.5	74.1	0.082	0.342	0.9647	0.0454	0.0342	0.35
77.5	82.5	78.1	−0.293	0.312	0.9778	0.0457	0.0211	0.87
22.5	27.5	25.8	0.270	0.899	0.9544	−0.1335	0.0359	0.15
27.5	32.5	30.6	−0.162	0.199	0.9683	−0.1346	0.0220	0.38
32.5	37.5	35.4	0.018	0.146	0.9713	−0.1348	0.0190	0.33
37.5	42.5	40.1	−0.079	0.098	0.9727	−0.1349	0.0176	0.75
42.5	47.5	44.9	0.011	0.100	0.9731	−0.1350	0.0172	0.59
47.5	52.5	49.8	0.308	0.149	0.9693	−0.1347	0.0210	0.39
52.5	57.5	55.4	0.007	0.106	0.9418	−0.1326	0.0485	0.72
57.5	62.5	60.0	0.041	0.082	0.9517	−0.1333	0.0385	0.22
62.5	67.5	64.9	0.009	0.112	0.9497	−0.1332	0.0406	0.64
67.5	72.5	69.8	0.114	0.175	0.9524	−0.1334	0.0379	0.46
72.5	77.5	74.1	−0.103	0.249	0.9629	−0.1342	0.0274	0.32
77.5	82.5	78.1	0.770	0.448	0.9744	−0.1351	0.0158	0.28
22.5	27.5	25.8	0.436	0.396	−0.0713	0.9590	0.0382	0.19
27.5	32.5	30.6	0.086	0.322	−0.0641	0.9666	0.0309	0.40
32.5	37.5	35.4	0.401	0.279	−0.0622	0.9682	0.0291	0.05
37.5	42.5	40.1	0.071	0.245	−0.0613	0.9690	0.0282	0.53
42.5	47.5	44.9	0.405	0.147	−0.0610	0.9692	0.0278	0.57
47.5	52.5	49.8	0.252	0.122	−0.0635	0.9671	0.0303	0.58
52.5	57.5	55.4	0.190	0.113	−0.0765	0.9523	0.0433	0.66
57.5	62.5	60.0	0.342	0.095	−0.0725	0.9576	0.0393	0.66
62.5	67.5	64.9	0.252	0.113	−0.0733	0.9565	0.0402	0.47
67.5	72.5	69.8	0.337	0.309	−0.0722	0.9580	0.0390	0.43
72.5	77.5	74.1	0.219	0.383	−0.0672	0.9636	0.0340	0.24
77.5	82.5	78.1	1.102	0.477	−0.0601	0.9700	0.0269	0.82
22.5	27.5	25.8	0.818	1.493	−0.0496	0.9595	0.0391	0.22
27.5	32.5	30.6	−0.092	0.291	−0.0420	0.9671	0.0316	0.28
32.5	37.5	35.4	0.280	0.247	−0.0401	0.9687	0.0296	0.34
37.5	42.5	40.1	0.137	0.181	−0.0391	0.9695	0.0287	0.46
42.5	47.5	44.9	0.506	0.170	−0.0388	0.9697	0.0283	0.43
47.5	52.5	49.8	0.189	0.215	−0.0414	0.9676	0.0309	0.27
52.5	57.5	55.4	0.332	0.195	−0.0551	0.9527	0.0446	0.53
57.5	62.5	60.0	0.217	0.140	−0.0508	0.9581	0.0404	0.34
62.5	67.5	64.9	0.138	0.175	−0.0517	0.9570	0.0413	0.59
67.5	72.5	69.8	0.120	0.288	−0.0505	0.9584	0.0400	0.59
72.5	77.5	74.1	−0.028	0.331	−0.0452	0.9641	0.0348	0.28
77.5	82.5	78.1	−0.599	1.006	−0.0378	0.9704	0.0274	0.36

$$\left[\frac{d\sigma}{d\Omega}\right]_{I=0}(\theta)=2\left[\frac{d\sigma}{d\Omega}\right]_{np}(\theta)+2\left[\frac{d\sigma}{d\Omega}\right]_{np}(\pi-\theta)-\left[\frac{d\sigma}{d\Omega}\right]_{pp}(\theta)\,, \tag{13}$$

$$\left[P\frac{d\sigma}{d\Omega}\right]_{I=0}(\theta)=2\left[P\frac{d\sigma}{d\Omega}\right]_{np}(\theta)-2\left[P\frac{d\sigma}{d\Omega}\right]_{np}(\pi-\theta)-\left[P\frac{d\sigma}{d\Omega}\right]_{pp}(\theta)\,, \tag{14}$$

TABLE V. Pure spin observables. The quantities $\theta_{\min}$, $\theta_{\max}$, and $\langle\theta_{\text{c.m.}}\rangle$ are in degrees and represent the boundaries and central value of the c.m. angle for each bin.

$\theta_{\min}$	$\theta_{\max}$	$\langle\theta_{\text{c.m.}}\rangle$	C_{SS}	ΔC_{SS}	C_{LS}	ΔC_{LS}	χ^2/N_{DF}
			$T=484$ MeV				
22.5	27.5	26.6	−0.012	0.336	−0.152	0.444	
27.5	32.5	30.6	0.172	0.528	0.345	0.310	
32.5	37.5	35.2	0.022	0.187	0.060	0.224	
37.5	42.5	40.1	0.083	0.087	0.048	0.089	
42.5	47.5	45.0	0.127	0.073	−0.082	0.068	
47.5	52.5	49.8	0.194	0.069	0.079	0.072	
52.5	57.5	55.2	0.046	0.086	−0.006	0.083	
57.5	62.5	60.3	0.144	0.065	−0.068	0.063	
62.5	67.5	65.0	0.046	0.061	0.039	0.060	
67.5	72.5	69.9	0.017	0.078	0.004	0.076	
72.5	77.5	74.7	−0.059	0.105	−0.038	0.106	
77.5	82.5	78.9	0.105	0.209	0.014	0.194	
			$T=634$ MeV				
22.5	27.5	25.8	−0.375	1.296	0.748	0.790	0.04
27.5	32.5	30.7	0.030	0.329	−0.045	0.318	0.76
32.5	37.5	35.4	−0.011	0.102	0.262	0.146	0.13
37.5	42.5	40.1	0.150	0.108	−0.026	0.094	1.59
42.5	47.5	45.0	0.067	0.077	−0.017	0.076	1.91
47.5	52.5	49.6	0.163	0.091	0.038	0.090	0.56
52.5	57.5	55.3	−0.110	0.152	−0.049	0.155	3.40
57.5	62.5	60.1	0.119	0.064	−0.088	0.063	2.30
62.5	67.5	64.9	0.077	0.088	−0.015	0.088	0.97
67.5	72.5	69.8	0.245	0.093	0.058	0.095	0.45
72.5	77.5	74.4	0.156	0.115	0.084	0.121	0.96
77.5	82.5	78.4	−0.323	0.309	−0.371	0.304	1.44
			$T=720$ MeV				
22.5	27.5	25.8	0.424	0.594	0.018	0.553	
27.5	32.5	30.6	−0.090	0.232	−0.032	0.511	
32.5	37.5	35.1	0.217	0.240	−0.184	0.178	
37.5	42.5	40.1	−0.117	0.185	0.107	0.124	
42.5	47.5	45.0	0.163	0.153	0.026	0.173	
47.5	52.5	49.8	−0.047	0.198	−0.385	0.200	
52.5	57.5	55.4	0.368	0.223	−0.037	0.252	
57.5	62.5	60.1	0.332	0.124	0.036	0.142	
62.5	67.5	64.9	0.204	0.158	−0.014	0.168	
67.5	72.5	69.8	0.218	0.210	0.047	0.249	
72.5	77.5	74.3	0.345	0.353	0.003	0.295	
77.5	82.5	78.3	−1.972	1.498	−0.479	0.957	
			$T=788$ MeV				
22.5	27.5	25.8	0.108	0.388	0.494	0.401	0.06
27.5	32.5	30.6	−0.164	0.156	−0.024	0.223	0.09
32.5	37.5	35.4	0.080	0.104	0.361	0.189	0.27
37.5	42.5	40.1	−0.107	0.071	0.089	0.148	0.25
42.5	47.5	44.9	0.047	0.064	0.444	0.114	0.71
47.5	52.5	49.8	0.234	0.091	0.243	0.109	0.30
52.5	57.5	55.4	0.000	0.074	0.220	0.103	0.22
57.5	62.5	60.0	0.024	0.057	0.304	0.082	0.55
62.5	67.5	64.9	0.093	0.078	0.227	0.099	0.30
67.5	72.5	69.8	0.191	0.137	0.238	0.219	0.20
72.5	77.5	74.1	−0.050	0.192	0.081	0.260	0.14
77.5	82.5	78.1	0.079	0.215	0.664	0.439	2.39

TABLE VI. Values of χ^2 per degree of freedom for various phase-shift and model predictions compared to the data in Table V. The results of Bugg's [34] predictions at 634 and 720 MeV are from an interpolation by Bryan *et al.* in the SAID computer program of Arndt *et al.* [31].

Parameter	Arndt *et al.* [12,31]	Bystricky, Lechanoine-Leluc, and Lehar [13]	Bugg [34]	Hoshizaki and co-workers [11]	Lee and co-workers [35]
484 MeV					
C_{SS}	0.44	1.07	0.69	0.63	1.18
C_{LS}	2.54	2.04	2.70	2.42	2.54
634 MeV					
C_{SS}	1.65	0.66	0.95	0.90	1.65
C_{LS}	1.71	2.09	1.56	0.66	1.26
720 MeV					
C_{SS}	0.61	0.79	1.23	2.35	
C_{LS}	0.89	0.99	0.86	1.42	
788 MeV					
C_{SS}	3.37	4.76	0.90	3.86	4.74
C_{LS}	2.93	2.13	2.87	3.45	4.22

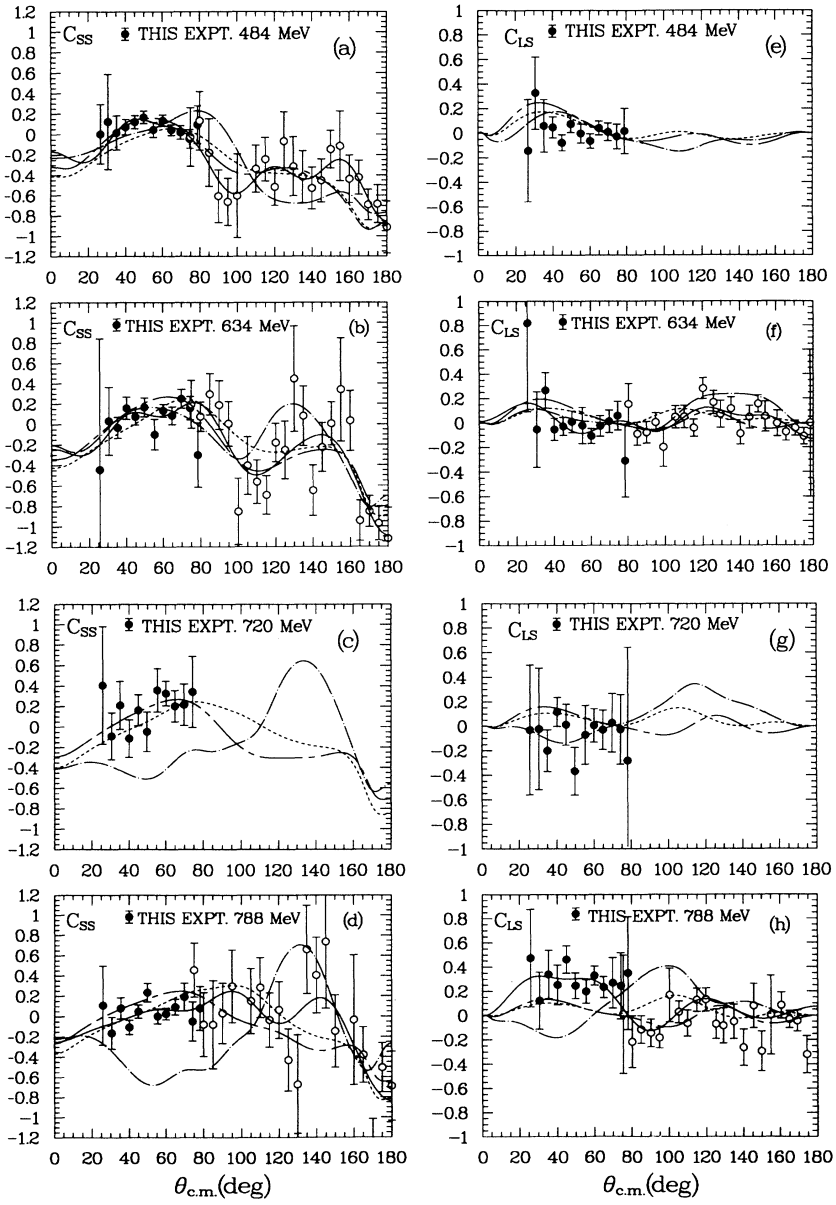

FIG. 8. Plots of the spin observables C_{SS} and C_{LS} at 484, 634, 720, and 788 MeV. Solid circles with error bars are the present data. Open circles with error bars are the data from the previous runs of these experiments (E665 and E770). Solid lines are fits to the experimental data. All other lines are PSA predictions; chain-dashed, dashed, and chain-dotted lines are from the PSA predictions of Arndt *et al.* [12,31], Bugg [34], and Hoshizaki and co-workers [33], respectively. The more recent PSA (Saclay [13] and Hoshizaki and co-workers [11]) and model (Lee and co-workers [35]) predictions are all similar to those of Arndt *et al.* and Bugg, while the prediction of Hoshizaki and co-workers shown is typical of older PSA's, before much of the recent data had been added to the *np* databases.

$$\left[C_{LS}\frac{d\sigma}{d\Omega}\right]_{I=0}(\theta)=2\left[C_{LS}\frac{d\sigma}{d\Omega}\right]_{np}(\theta)-2\left[C_{LS}\frac{d\sigma}{d\Omega}\right]_{np}(\pi-\theta)-\left[C_{LS}\frac{d\sigma}{d\Omega}\right]_{pp}(\theta)\,, \tag{15}$$

$$\left[C_{\alpha\alpha}\frac{d\sigma}{d\Omega}\right]_{I=0}(\theta)=2\left[C_{\alpha\alpha}\frac{d\sigma}{d\Omega}\right]_{np}(\theta)+2\left[C_{\alpha\alpha}\frac{d\sigma}{d\Omega}\right]_{np}(\pi-\theta)-\left[C_{\alpha\alpha}\frac{d\sigma}{d\Omega}\right]_{pp}(\theta)\,, \tag{16}$$

where α indicates the polarization direction (N, L, or S) of the beam and target. Note here that both $(d\sigma/d\Omega)_{I=0}$ and $(C_{\alpha\alpha}\,d\sigma/d\Omega)_{I=0}$ are symmetric about $\theta=90°$.

Figure 9 shows $(C_{LS}\,d\sigma/d\Omega)_{I=0}$ and $(C_{SS}\,d\sigma/d\Omega)_{I=0}$ at 484, 634, and 788 MeV. Differences in shape are noted for both quantities as a function of energy. The $I=1$ spin observables and np differential cross sections were taken from the SM89 phase-shift predictions of Arndt *et al.* [31], and the np data for C_{LS} and C_{SS} for c.m. angles between 80° and 155° are from Refs. [6] and [7], respectively. The error bars shown in Fig. 9 are from statistical uncertainties on the np data for C_{LS} and C_{SS} only.

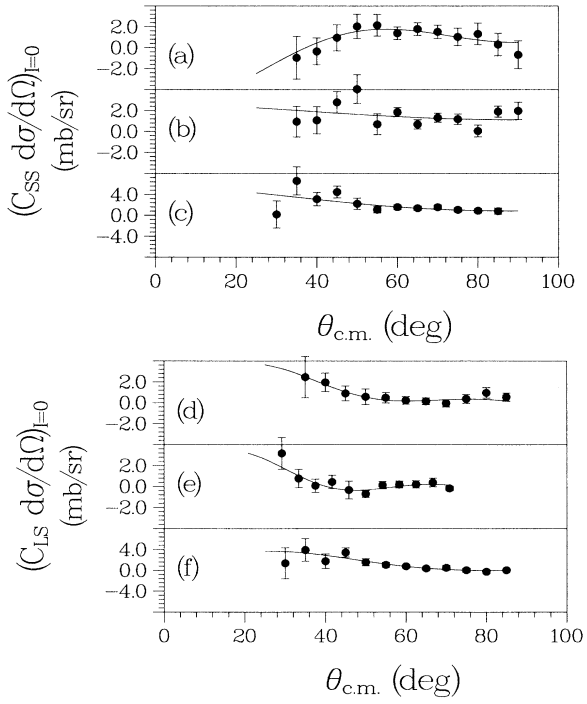

FIG. 9. Plots of the quantities $(C_{SS}\,d\sigma/d\Omega)_{I=0}$ and $(C_{LS}\,d\sigma/d\Omega)_{I=0}$ from the data in this paper combined with other results [6,7,31]. Data are presented for (a), (d) 484 MeV, (b), (e) 634 MeV, and (c), (f) 788 MeV as a function of c.m. scattering angle. The curves are Legendre and associated Legendre polynomial fits as described in the text.

The $(C_{LS}\,d\sigma/d\Omega)_{I=0}$ and $(C_{SS}\,d\sigma/d\Omega)_{I=0}$ results were fitted, respectively, with associated and regular Legendre polynomials of even order. Three terms were used in all fits, and the results are shown in Fig. 9. In general, the coefficients of the higher-order terms show less energy dependence than the lower-order coefficients. However, the uncertainties on the higher-order coefficients are particularly large for the $(C_{SS}\,d\sigma/d\Omega)_{I=0}$ data.

A Legendre analysis of the partial waves contributing to $(C_{LS}\,d\sigma/d\Omega)_{I=0}$ and $(C_{SS}\,d\sigma/d\Omega)_{I=0}$ was performed. Spin-singlet partial waves, such as $^1P_1$ and $^1F_3$, cannot contribute to $C_{LS}\,d\sigma/d\Omega$. Also, partial waves with higher J contribute to the higher-order Legendre polynomial coefficients, whereas waves with small J do not. The results suggest that the observed variation is consistent with changes in the $^3D_1$ wave if only one partial wave is responsible. On the other hand, there are insufficient statistics to rule out other (especially higher-order) waves, nor can the case with energy variation in more than one partial wave be rejected.

A set of spin observables that correspond purely to an interference of amplitudes for $I=0$ and 1 can also be defined [37]:

$$\left[\frac{d\sigma}{d\Omega}\right]_{\rm int}(\theta)=2\left[\frac{d\sigma}{d\Omega}\right]_{np}(\theta)-2\left[\frac{d\sigma}{d\Omega}\right]_{np}(\pi-\theta)\,, \tag{17}$$

$$\left[P\frac{d\sigma}{d\Omega}\right]_{\rm int}(\theta)=2\left[P\frac{d\sigma}{d\Omega}\right]_{np}(\theta)+2\left[P\frac{d\sigma}{d\Omega}\right]_{np}(\pi-\theta)\,, \tag{18}$$

$$\left[C_{LS}\frac{d\sigma}{d\Omega}\right]_{\rm int}(\theta)=2\left[C_{LS}\frac{d\sigma}{d\Omega}\right]_{np}(\theta)+2\left[C_{LS}\frac{d\sigma}{d\Omega}\right]_{np}(\pi-\theta)\,, \tag{19}$$

$$\left[C_{\alpha\alpha}\frac{d\sigma}{d\Omega}\right]_{\rm int}(\theta)=2\left[C_{\alpha\alpha}\frac{d\sigma}{d\Omega}\right]_{np}(\theta)-2\left[C_{\alpha\alpha}\frac{d\sigma}{d\Omega}\right]_{np}(\pi-\theta)\,, \tag{20}$$

where α refers to N, L, or S as before.

Figure 10 shows $(C_{LS}\,d\sigma/d\Omega)_{\rm int}$ and $(C_{SS}\,d\sigma/d\Omega)_{\rm int}$ calculated using the same data as for Fig. 9. Fits with odd order associated and regular Legendre polynomials are also given. Again, the coefficients of the higher-order terms show less energy dependence than the lower-order coefficients.

A unique determination of the pp amplitudes, aside from an overall phase, requires at least 11 different experiments [38] since the amplitudes are complex and bilin-

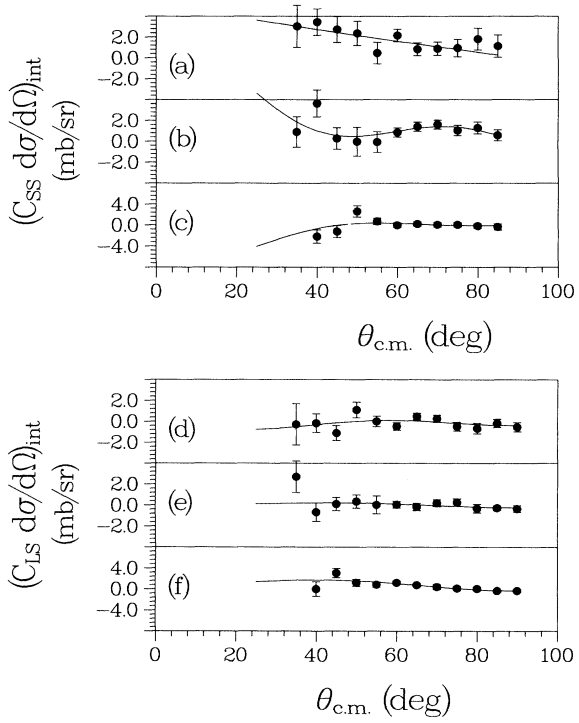

FIG. 10. Plots of the quantities $(C_{SS}\, d\sigma/d\Omega)_{int}$ and $(C_{LS}\, d\sigma/d\Omega)_{int}$ from the data in this paper combined with other results [6,7,31]. Data are presented for (a), (d) 484 MeV, (b), (e) 634 MeV, and (c), (f) 788 MeV as a function of c.m. scattering angle. The curves are Legendre and associated Legendre polynomial fits as described in the text.

early related to the observables. Assuming that the $I=1$ (pp) amplitudes are known, at least the same number of np experiments are needed to determine the $I=0$ amplitudes, although np scattering experiments at θ and $\pi-\theta$ can be counted as independent. Thus, for $I=0$, to solve for all the amplitudes up to some discrete ambiguities, only six observables need to be measured over the entire angular region $0<\theta<180°$. Furthermore, it has been shown recently [37] that the number of observables required for a *unique* determination of the $I=0$ amplitudes (up to an arbitrary, overall phase) is 8, where these are $d\sigma/d\Omega$, P, C_{LS}, C_{NN}, C_{SS}, C_{LL}, D_{NN}, and K_{NN}. Only the modulus of each amplitude [37] can be determined at present from the results of this series of experiments $(C_{LL}, C_{NN}, C_{SS}, C_{LS})$.

However, existing data and measurements in progress at LAMPF will permit a full $I=0$ amplitude reconstruction in the near future. Other elastic-scattering observables measured between 400 and 900 MeV include free np differential cross sections [39–52], polarizations [53–60], and other spin observables [5–8,54–56,59,61–63]. Many of these data are at backward c.m. angles, and there are some inconsistencies that may eventually limit the knowledge of the amplitudes. The inconsistencies in the polarization data (see Ref. [59]) may be clarified by new measurements in progress at LAMPF. There are also discrepancies among various backward differential cross-section data (see Refs. [46] and [48]). In addition to the free np results, np quasielastic (pd) scattering measurements exist in this same energy region for differential cross sections [64–66], polarizations [66–79], and other spin observables [8,19,20,69–71,76,78–82]. Comparison of free and quasielastic spin observable data for pp elastic scattering frequently shows good agreement. This suggests that both the free np elastic and np quasielastic measurements will be very helpful in the amplitude determination.

The data presented in this paper provide substantial input to the nucleon-nucleon database and will go far toward a model-independent determination of the amplitudes for discrete energies between 450 and 800 MeV, as well as the establishment of a unique phase-shift solution in the $I=0$ channel in this energy range.

ACKNOWLEDGMENTS

We thank the staff at LAMPF for providing the polarized proton beam and the polarized target group for the target used in this experiment. We also wish to acknowledge the assistance of D. Lopiano with some of the figures and of M. McNaughton with the determination of the proton-beam polarization direction. This experiment was supported in part by the U.S. Department of Energy, Contracts Nos. W-31-109-ENG-38 and DE-AS05-76ER04449 and Grants Nos. DE-FG05-88ER40399 and DE-FG04-88ER40403, and by Associated Western Universities.

[1] There are 16 helicity amplitudes, but only five of them are independent. See, for example, M. L. Goldberger, M. T. Grisaru, S. W. MacDowell, and D. Y. Wong, Phys. Rev. **120**, 2250 (1960); A. Scotti and D. Y. Wong, *ibid.* **138**, B145 (1965). The *NN* scattering matrix is constructed such that it is invariant under space rotations, space reflections, and time reversal; see L. Wolfenstein and J. Ashkin, *ibid.* **85**, 947 (1952).

[2] J. Bystricky, F. Lehar, and P. Winternitz, J. Phys. (Paris) **39**, 1 (1978); G. H. Thomas, Ph.D. thesis, University of California, Los Angeles, 1969. For some derivations of the observables, see G. L. Kane and U. P. Sukhatme, Nucl. Phys. **B78**, 110 (1974).

[3] I. P. Auer, J. Chalmers, E. Colton, R. Giese, H. Halpern, D. Hill, R. Miller, K. Nield, B. Sandler, H. Spinka, N. Tamura, D. Underwood, Y. Watanabe, A. Yokosawa, A. Beretvas, and D. Miller, Phys. Rev. D **32**, 1609 (1985).

[4] For a summary of the formalism, see N. Hoshizaki, Prog. Theor. Phys. Suppl. **42**, 107 (1968); R. A. Arndt and L. D. Roper, Phys. Rev. D **25**, 2011 (1982); R. A. Arndt, L. D. Roper, R. A. Bryan, R. B. Clark, B. J. VerWest, and P. Signell, *ibid.* **28**, 97 (1983).

[5] G. R. Burleson, J. A. Faucett, C. A. Fontenla, R. W. Garnett, M. W. Rawool, W. R. Ditzler, D. Hill, J. Hoftiezer,

K. F. Johnson, D. Lopiano, T. Shima, H. Shimizu, H. Spinka, R. Stanek, D. Underwood, R. Wagner, A. Yokosawa, T. S. Bhatia, G. Glass, J. C. Hiebert, R. A. Kenefick, S. Nath, L. C. Northcliffe, R. Damjanovich, J. J. Jarmer, R. H. Jeppesen, and G. E. Tripard, Phys. Rev. Lett. **59**, 1645 (1987).

[6] W. R. Ditzler, D. Hill, J. Hoftiezer, K. F. Johnson, D. Lopiano, T. Shima, H. Shimizu, H. Spinka, R. Stanek, D. Underwood, R. G. Wagner, A. Yokosawa, G. R. Burleson, J. A. Faucett, C. A. Fontenla, R. W. Garnett, C. Luchini, M. W. Rawool-Sullivan, T. S. Bhatia, G. Glass, J. C. Hiebert, R. A. Kenefick, S. Nath, L. C. Northcliffe, R. Damjanovich, J. J. Jarmer, J. Vaninetti, R. H. Jeppesen, and G. E. Tripard, Phys. Rev. D **46**, 2792 (1992).

[7] R. Garnett, M. Rawool, V. Carlson, D. Hill, K. F. Johnson, D. Lopiano, Y. Ohashi, T. Shima, H. Spinka, R. Stanek, D. Underwood, A. Yokosawa, M. Beddo, G. Burleson, J. A. Faucett, G. Kyle, H. Shimizu, G. Glass, S. Nath, L. C. Northcliffe, J. J. Jarmer, R. H. Jeppesen, and G. E. Tripard, Phys. Rev. D **40**, 1708 (1989).

[8] M. W. McNaughton, K. Koch, I. Supek, N. Tanaka, K. H. McNaughton, P. J. Riley, D. A. Ambrose, J. D. Johnson, A. Smith, G. Glass, J. C. Hiebert, L. C. Northcliffe, A. J. Simon, D. L. Adams, R. D. Ransome, D. B. Clayton, H. M. Spinka, R. H. Jeppesen, and G. E. Tripard, Phys. Rev. C **44**, 2267 (1991); M. W. McNaughton, K. Koch, I. Supek, N. Tanaka, D. A. Ambrose, P. Coffey, K. Johnston, K. H. McNaughton, P. J. Riley, G. Glass, J.C. Hiebert, L. C. Northcliffe, A. J. Simon, D. J. Mercer, D. L. Adams, H. Spinka, R. H. Jeppesen, G. E. Tripard, and H. Woolverton, *ibid.* **45**, 2564 (1992); K. H. McNaughton, D. A. Ambrose, P. Coffey, K. Johnston, P. J. Riley, M. W. McNaughton, K. Koch, I. Supek, N. Tanaka, G. Glass, J. C. Hiebert, L. C. Northcliffe, A. J. Simon, D. J. Mercer, D. L. Adams, H. Spinka, R. H. Jeppesen, G. E. Tripard, and H. Woolverton, *ibid.* **46**, 47 (1992).

[9] For example, M. P. Locher, M. E. Sainio, and A. Svarc, Adv. Nucl. Phys. **17**, 47 (1986); A. Yokosawa, J. Phys. Soc. Jpn. Suppl. **55**, 251 (1986); T. Shima, in *Panic '87,* Proceedings of the Eleventh International Conference on Particles and Nuclei, Kyoto, Japan, 1987, edited by S. Homma *et al.* [Nucl. Phys. **A478**, 543c (1988)].

[10] N. Hoshizaki, Prog. Theor. Phys. **60**, 1796 (1978); **61**, 129 (1979).

[11] Y. Higuchi, N. Hoshizaki, H. Masuda, and H. Nakao, Prog. Theor. Phys. **86**, 17 (1991); N. Hoshizaki and T. Watanabe, *ibid.* **86**, 321 (1991); **86**, 327 (1991).

[12] R. A. Arndt, J. S. Hyslop, and L. D. Roper, Phys. Rev. D **35**, 128 (1987); R. A. Arndt, L. D. Roper, R. L. Workman, and M. W. McNaughton, *ibid.* **45**, 3995 (1992).

[13] J. Bystricky, C. Lechanoine-Leluc, and F. Lehar, J. Phys. (Paris) **48**, 199 (1987); **51**, 2747 (1990).

[14] A. Yokosawa, Phys. Rep. **64**, 47 (1980), for a summary of early results.

[15] F. Lehar, A. de Lesquen, L. van Rossum, P. Chaumette, J. Deregel, J. Fabre, M. de Mali, J. M. Fontaine, D. Legrand, F. Perrot, J. Ball, C. D. Lac, P. Bach, G. Gaillard, R. Hess, Ph. Sormani, V. Ghazikhanian, C. A. Whitten, R. Peschina, and E. Rossle, Phys. Lett. B **189**, 241 (1987); R. Binz, B. van den Brandt, R. Buchle, M. Daum, Ph. Demierre, J. Franz, G. Gaillard, N. Hamann, R. Hess, J. A. Konter, F. Lehar, C. Lechanoine-Leluc, S. Mango, R. Peschina, D. Rapin, E. Rossle, P. A. Schmelzbach, H. Schmitt, and R. Todenhagen, in *Proceedings of the Twelfth International Conference on Few Body Problems,* Vancouver, British Columbia, 1989, edited by H. W. Fearing [Nucl. Phys. **A508**, 267c (1990)]; M. Beddo, G. Burleson, J. A. Faucett, S. Gardiner, G. Kyle, R. Garnett, D. P. Grosnick, D. Hill, K. F. Johnson, D. Lopiano, Y. Ohashi, T. Shima, H. Spinka, R. Stanek, D. Underwood, A. Yokosawa, G. Glass, R. Kenefick, S. Nath, L. Northcliffe, J. J. Jarmer, S. Pentilla, R. H. Jeppesen, G. Tripard, M. Devereux, and P. Kroll, Phys. Lett. B **258**, 24 (1991); J. M. Fontaine, F. Perrot-Kunne, J. Bystricky, F. Lehar, A. de Lesquen, M. de Mali, L. van Rossum, J. Ball, Ph. Chesny, C. D. Lac, J. L. Sans, J. P. Goudour, P. Bach, G. Gaillard, R. Hess, R. Kunne, D. Rapin, Ph. Sormani, R. Binz, A. Klett, R. Peschina, E. Rossle, and H. Schmitt, Nucl. Phys. **B358**, 297 (1991).

[16] Many theoretical papers on dibaryons have been published, for example, P. J. G. Mulders, A. Th. M. Aerts, and J. J. de Swart, Phys. Rev. Lett. **40**, 1543 (1978); E. L. Lomon, in *Proceedings of the Tenth International Conference on Particles and Nuclei,* Heidelberg, Germany, 1984, edited by B. Povh and G. Zu Putlitz [Nucl. Phys. **A434**, 139c (1985)]; T. Goldman, K. Maltman, G. J. Stephenson, K. E. Schmidt, and F. Wang, Phys. Rev. C **39**, 1889 (1989); N. Konno, H. Nakamura, and H. Noya, Phys. Rev. D **35**, 239 (1987).

[17] C. W. Bjork, P. J. Riley, B. E. Bonner, J. E. Simmons, K. D. Williamson, M. L. Evans, G. Glass, J. C. Hiebert, M. Jain, R. A. Kenefick, L. C. Northcliffe, C. G. Cassapakis, H. C. Bryant, B. D. Dieterle, C. P. Leavitt, D. M. Wolfe, and D. W. Werren, Phys. Lett. **63B**, 31 (1976).

[18] C. W. Bjork, Ph.D. thesis, University of Texas at Austin, Los Alamos National Laboratory Report No. LA-6192-T, 1976 (unpublished).

[19] P. J. Riley, C. L. Hollas, C. R. Newsom, R. D. Ransome, B. E. Bonner, J. E. Simmons, T. S. Bhatia, G. Glass, J. C. Hiebert, L. C. Northcliffe, and W. B. Tippens, Phys. Lett. **103B**, 313 (1981).

[20] J. S. Chalmers, W. R. Ditzler, T. Shima, H. Shimizu, H. Spinka, R. Stanek, D. Underwood, R. Wagner, A. Yokosawa, J. E. Simmons, G. Burleson, C. Fontenla, T. S. Bhatia, G. Glass, and L. C. Northcliffe, Phys. Lett. **153B**, 235 (1985).

[21] M. W. McNaughton, P. R. Bevington, H. B. Willard, E. Winkelmann, E. P. Chamberlin, F. H. Cverna, N. S. P. King, and H. Willmes, Phys. Rev. C **23**, 1128 (1981).

[22] M. W. McNaughton, Los Alamos National Laboratory Report No. LA-8307-MS, 1980 (unpublished).

[23] C. L. Hollas, R. D. Ransome, P. J. Riley, B. E. Bonner, J. G. Boissevain, T. S. Bhatia, G. Glass, J. C. Hiebert, and W. B. Tippens, Nucl. Instrum. Methods A **219**, 275 (1984).

[24] H. Spinka, Argonne National Laboratory Report No. ANL-HEP-TR-88-14, 1988 (unpublished).

[25] P. Autones, J. C. Brisson, A. Boucherie, G. Cozzika, J. Deregel, J. P. Duthil, H. Desportes, Y. Ducros, A. Katz, A. de Lesquen, J. P. Merlo, J. F. Mougel, J. Movchet, J. C. Raoul, B. Tasi, L. van Rossum, B. Amblard, J. M. Fontaine, M. Hansroul, and J. M. Rieubland, Nucl. Instrum. Methods **103**, 211 (1972).

[26] J. C. Raoul, P. Autones, R. Auzolle, C. Bruneton, J. Bystricky, G. Cozzika, J. Deregel, Y. Ducros, A. Gaidot, A. Katz, F. Khantine-Langlois, F. Lehar, A. de Lesquen, J. P. Merlo, S. Miyashita, J. Movchet, J. Pierrard, M. Ramadier, P. Roubeau, G. Souchere, L. van Rossum, A. A.

Derevschikov, N. I. Golovnya, Yu. S. Khoderev, Yu. A. Matulenko, A. P. Meschanin, S. B. Nurushev, A. I. Saraykin, V. S. Seleznev, V. V. Siksin, E. V. Smirnov, V. L. Solovyanov, V. N. Zapolsky, Yu. M. Kazarinov, M. Yu. Kazarinov, B. A. Khatchaturov, I. K. Potashnikova, and V. P. Kanavets, Nucl. Instrum. Methods **125**, 585 (1975).

[27] I. P. Auer, W. R. Ditzler, D. Hill, K. Imai, H. Spinka, R. Stanek, K. Toshioka, D. Underwood, R. Wagner, A. Yokosawa, E. W. Hoffman, J. J. Jarmer, G. R. Burleson, W. B. Cottingame, S. J. Greene, and S. Stuart, Phys. Rev. D **29**, 2435 (1984).

[28] A. Abragam and M. Goldman, *Nuclear Magnetism: Order and Disorder* (Clarendon, Oxford, 1982); Rep. Prog. Phys. **41**, 395 (1978).

[29] W. Haberichter, T. Kasprzyk, H. Shimizu, H. Spinka, R. Stanek, G. Burleson, R. Garnett, and J. Tobin, Nucl. Instrum. Methods A **270**, 361 (1988).

[30] For the experiment in Ref. [7], $P3$ had individual readouts for each wire, while this experiment had delay-line cards for groups of 16 wires. No $P0$ and $P3$ chambers were used for the experiment in Refs. [5] and [6].

[31] The PSA predictions were obtained from the SAID program by R. Arndt *et al.*, available at Virginia Polytechnic Institute and State University and at LAMPF. The SM89 solutions are used in the plots. Note that the spin observable AZX calculated in the SAID computer program is $-C_{LS}=-C_{SL}$ as defined in this paper.

[32] R. W. Garnett, Ph.D. thesis, New Mexico State University, Los Alamos National Laboratory Report No. LA-11491-T, 1989 (unpublished).

[33] K. Hashimoto, Y. Higuchi, and N. Hoshizaki, Prog. Theor. Phys. **64**, 1678 (1980); K. Hashimoto and N. Hoshizaki, *ibid.* **64**, 1693 (1980).

[34] R. Dubois, D. Axen, R. Keeler, M. Comyn, G. A. Ludgate, J. R. Richardson, N. M. Stewart, A. S. Clough, D. V. Bugg, and J. A. Edgington, Nucl. Phys. **A377**, 554 (1982); D. V. Bugg, Phys. Rev. C **41**, 2708 (1990).

[35] M. Betz and T.-S. H. Lee, Phys. Rev. C **23**, 375 (1981); T.-S. H. Lee, Phys. Rev. Lett. **50**, 1571 (1983); Phys. Rev. C **29**, 195 (1984); T.-S. H. Lee and A. Matsuyama, *ibid.* **32**, 1986 (1985); **36**, 1459 (1987); T.-S. H. Lee (private communication).

[36] P. R. Bevington, *Data Reduction and Error Analysis for the Physical Sciences* (McGraw-Hill, New York, 1969).

[37] H. Spinka, Phys. Rev. D **30**, 1461 (1984).

[38] C. R. Schumacher and H. A. Bethe, Phys. Rev. **121**, 1534 (1961). See also Ref. [3].

[39] A. J. Hartzler and R. T. Siegel, Phys. Rev. **95**, 185 (1954); A. J. Hartzler, R. T. Siegel, and W. Opitz, *ibid.* **95**, 591 (1954).

[40] Yu. M. Kazarinov and Yu. N. Simonov, Zh. Eksp. Teor. Fiz. **31**, 169 (1956) [Sov. Phys. JETP **4**, 161 (1957)].

[41] N. S. Amaglobeli and Yu. M. Kazarinov, Zh. Eksp. Teor. Fiz. **33**, 53 (1958) [Sov. Phys. JETP **7**, 37 (1958)]; **37**, 1587 (1959) [**10**, 1125 (1960)].

[42] B. M. Golovin, V. P. Dzhelepov, Yu. V. Katyshev, A. D. Konin, and S. V. Medved, Zh. Eksp. Teor. Fiz. **36**, 735 (1959) [Sov. Phys. JETP **9**, 516 (1959)].

[43] R. R. Larsen, Nuovo Cimento **18**, 1039 (1960).

[44] P. F. Shepard, T. J. Devlin, R. E. Mischke, and J. Solomon, Phys. Rev. D **10**, 2735 (1974).

[45] G. Bizard, F. Bonthonneau, J. L. Laville, F. Lefebvres, J. C. Malherbe, R. Regimbart, J. Duflo, and F. Plouin, Nucl. Phys. **B85**, 14 (1975).

[46] B. E. Bonner, J. E. Simmons, C. L. Hollas, C. R. Newsom, P. J. Riley, G. Glass, and M. Jain, Phys. Rev. Lett. **41**, 1200 (1978).

[47] R. Carlini, B. Dieterle, J. Donahue, C. Leavitt, T. Rupp, W. Thomas, D. Wolfe, L. B. Auerbach, V. L. Highland, K. F. Johnson, W. K. McFarlane, J. Pratt, and R. Bentley, Phys. Rev. Lett. **41**, 1341 (1978).

[48] W. Hurster, Th. Fischer, G. Hammel, K. Kern, M. Kleinschmidt, L. Lehmann, H. Schmitt, L. Schmitt, and D. M. Sheppard, Phys. Lett. **90B**, 367 (1980).

[49] M. L. Evans, G. Glass, J. C. Hiebert, M. Jain, R. A. Kenefick, L. C. Northcliffe, B. E. Bonner, J. E. Simmons, C. W. Bjork, P. J. Riley, H. C. Bryant, C. G. Cassapakis, B. Dieterle, C. P. Leavitt, D. M. Wolfe, and D. W. Werren, Phys. Rev. C **26**, 2525 (1982).

[50] R. K. Keeler, R. Dubois, E. G. Auld, D. A. Axen, M. Comyn, G. Ludgate, L. P. Robertson, J. R. Richardson, D. V. Bugg, J. A. Edgington, W. R. Gibson, A. S. Clough, N. M. Stewart, and B. Dieterle, Nucl. Phys. **A377**, 529 (1982).

[51] M. Jain, M. L. Evans, G. Glass, J. C. Hiebert, R. A. Kenefick, L. C. Northcliffe, B. E. Bonner, J. E. Simmons, C. W. Bjork, P. J. Riley, H. C. Bryant, C. G. Cassapakis, B. Dieterle, C. P. Leavitt, D. M. Wolfe, and D. W. Werren, Phys. Rev. C **30**, 566 (1984).

[52] Y. Terrien, J. C. Lugol, J. Saudinos, B. H. Silverman, F. Wellers, G. A. Korolev, A. V. Dobrovolsky, A. V. Khanzadeev, G. E. Petrov, E. M. Spiridenkov, and A. A. Vorobyov, Phys. Rev. Lett. **59**, 1534 (1987).

[53] P. R. Robrish, O. Chamberlain, R. D. Field, R. Z. Fuzesy, W. Gorn, C. C. Morehouse, T. Powell, S. Rock, S. Shannon, G. Shapiro, H. Weisberg, and M. J. Longo, Phys. Lett. **31B**, 617 (1970).

[54] A. S. Clough, D. R. Gibson, D. Axen, R. Dubois, L. Felawka, R. Keeler, G. A. Ludgate, C. J. Oram, C. Amsler, D. V. Bugg, J. A. Edgington, L. P. Robertson, N. M. Stewart, J. Beveridge, and J. R. Richardson, Phys. Rev. C **21**, 988 (1980).

[55] Yu. S. Bagaturiya, Yu. M. Kazarinov, M. Yu. Kazarinov, M. Yu. Liburg, V. N. Matafonov, G. G. Macharashvili, I. K. Potashnikova, I. Strakhota, M. Strakhotova, Yu. A. Usov, B. A. Khachaturov, and M. R. Khayatov, Yad. Fiz. **33**, 1237 (1981) [Sov. J. Nucl. Phys. **33**, 659 (1981)].

[56] R. D. Ransome, C. L. Hollas, P. J. Riley, B. E. Bonner, W. R. Gibbs, M. W. McNaughton, J. E. Simmons, T. S. Bhatia, G. Glass, J. C. Hiebert, L. C. Northcliffe, and W. B. Tippens, Phys. Rev. Lett. **48**, 781 (1982).

[57] G. A. Korolev, A. V. Khanzadeev, G. E. Petrov, E. M. Spiridenkov, A. A. Vorobyov, Y. Terrien, J. C. Lugol, J. Saudinos, B. H. Silverman, and F. Wellers, Phys. Lett. **165B**, 262 (1985).

[58] C. R. Newsom, C. L. Hollas, R. D. Ransome, P. J. Riley, B. E. Bonner, J. G. J. Boissevain, J. J. Jarmer, M. W. McNaughton, J. E. Simmons, T. S. Bhatia, G. Glass, J. C. Hiebert, L. C. Northcliffe, and W. B. Tippens, Phys. Rev. C **39**, 965 (1989).

[59] D. Bandyopadhyay, R. Abegg, M. Ahmad, J. Birchall, K. Chantziantoniou, C. A. Davis, N. E. Davison, P. P. J. Delheij, P. W. Green, L. G. Greeniaus, D. C. Healey, C. Lapointe, W. J. McDonald, C. A. Miller, G. A. Moss, S. A. Page, W. D. Ramsay, N. L. Rodning, G. Roy, W. T. H. van Oers, G. D. Wait, J. W. Watson, and Y. Ye, Phys. Rev. C **40**, 2684 (1989).

[60] G. Glass, T. S. Bhatia, J. C. Hiebert, R. A. Kenefick, S.

Nath, L. C. Northcliffe, K. F. Johnson, H. Spinka, R. Stanek, M. W. Rawool, J. A. Faucett, R. H. Jeppesen, G. E. Tripard, and C. R. Newsom, Phys. Rev. C **41**, 2732 (1990).

[61] D. Axen, R. Dubois, R. Keeler, G. A. Ludgate, C. J. Oram, L. P. Robertson, N. M. Stewart, C. Amsler, D. V. Bugg, J. A. Edgington, W. R. Gibson, N. Wright, and A. S. Clough, Phys. Rev. C **21**, 998 (1980).

[62] J. Ball, C. D. Lac, F. Lehar, A. de Lesquen, L. van Rossum, P. Chaumette, J. Deregel, J. Fabre, M. de Mali, J. M. Fontaine, F. Perrot, P. Bach, G. Gaillard, R. Hess, D. Rapin, Ph. Sormani, V. Ghazikhanian, C. A. Whitten, R. Peschina, and E. Rossle, Z. Phys. C **40**, 193 (1988).

[63] S. Nath, G. Glass, J. C. Hiebert, J. A. Holt, R. A. Kenefick, L. C. Northcliffe, D. P. Grosnick, D. Lopiano, Y. Ohashi, T. Shima, H. M. Spinka, R. Stanek, T. S. Bhatia, J. J. Jarmer, P. J. Riley, S. Sen, J. A. Faucett, G. Kyle, R. H. Jeppesen, and G. E. Tripard, Phys. Rev. D **39**, 3520 (1989).

[64] G. Martelli, H. B. van der Raay, R. Rubinstein, K. R. Chapman, J. D. Dowell, W. R. Frisken, B. Musgrave, and D. H. Reading, Nuovo Cimento **21**, 581 (1961).

[65] L. M. C. Dutton and H. B. van der Raay, Phys. Rev. Lett. **21**, 1416 (1968).

[66] M. L. Barlett, G. W. Hoffmann, J. A. McGill, B. Hoistad, L. Ray, R. W. Fergerson, E. C. Milner, J. A. Marshall, J. F. Amann, B. E. Bonner, J. B. McClelland, G. S. Blanpied, and R. A. Arndt, Phys. Rev. C **27**, 682 (1983).

[67] B. M. Golovin, V. P. Dzhelepov, V. S. Nadezhdin, and V. I. Satarov, Zh. Eksp. Teor. Fiz. **36**, 433 (1959) [Sov. Phys. JETP **9**, 302 (1959)].

[68] D. Cheng, B. MacDonald, J. A. Helland, and P. M. Ogden, Phys. Rev. **163**, 1470 (1967).

[69] Yu. M. Kazarinov, F. Lehar, A. F. Pisarev, and Z. Janout, Yad. Fiz. **5**, 140 (1967) [Sov. J. Nucl. Phys. **5**, 97 (1967)].

[70] S. C. Wright, D. Shawhan, L. Pondrom, S. Olsen, and R. Handler, Phys. Rev. **175**, 1704 (1968).

[71] S. I. Bilenkaya, L. N. Gronti, Yu. M. Kazarinov, and V. S. Kiselev, Zh. Eksp. Teor. Fiz. **59**, 1049 (1970) [Sov. Phys. JETP **32**, 569 (1971)].

[72] R. Zulkarneev, Kh. Murtazaev, and V. Khachaturov, Phys. Lett. **61B**, 164 (1976).

[73] M. Sakuda, S. Isagawa, S. Ishimoto, S. Kabe, A. Masaike, K. Morimoto, K. Ogawa, M. Suetake, F. Takasaki, Y. Watase, N. Kim, S. Kobayashi, A. Murakami, A. de Lesquen, K. Nakajima, S. Nakada, T. Wada, and I. Yamauchi, Phys. Rev. D **25**, 2004 (1982).

[74] T. S. Bhatia, G. Glass, J. C. Hiebert, L. C. Northcliffe, W. B. Tippens, B. E. Bonner, J. E. Simmons, C. L. Hollas, C. R. Newsom, P. J. Riley, and R. D. Ransome, Phys. Rev. Lett. **48**, 227 (1982).

[75] J. Bystricky, J. Deregel, F. Lehar, A. de Lesquen, L. van Rossum, J. M. Fontaine, F. Perrot, J. Arvieux, T. Hasegawa, C. R. Newsom, Y. Onel, A. Penzo, H. Azaiez, A. Michalowicz, and C. Raymond, Nucl. Phys. **A444**, 597 (1985).

[76] J. A. Marshall, M. L. Barlett, R. W. Fergerson, G. W. Hoffmann, E. C. Milner, L. Ray, J. F. Amann, B. E. Bonner, and J. B. McClelland, Phys. Rev. C **34**, 1433 (1986).

[77] J. Ball, V. Ghazikhanian, J. Gordon, F. Lehar, A. de Lesquen, F. Perrot, and L. van Rossum, Nucl. Phys. **B286**, 635 (1987).

[78] A. de Lesquen, F. Lehar, L. van Rossum, P. Chaumette, J. Deregel, J. Fabre, J. M. Fontaine, F. Perrot, P. Bach, R. Hess, Ph. Sormani, J. Ball, C. D. Lac, D. Adams, J. Bystricky, V. Ghazikhanian, and C. A. Whitten, Nucl. Phys. **B304**, 673 (1988).

[79] M. L. Barlett, G. W. Hoffmann, L. Ray, G. Pauletta, K. H. McNaughton, J. F. Amann, K. W. Jones, J. B. McClelland, M. W. McNaughton, R. Fergerson, and D. Lopiano, Phys. Rev. C **40**, 2697 (1989).

[80] L. N. Gronti, Yu. M. Kazarinov, and M. R. Khayatov, Zh. Eksp. Teor. Fiz. **62**, 1998 (1972) [Sov. Phys. JETP **35**, 1042 (1972)].

[81] M. L. Barlett, G. W. Hoffmann, J. A. McGill, B. Hoistad, L. Ray, R. W. Fergerson, E. C. Milner, J. A. Marshall, J. F. Amann, B. E. Bonner, and J. B. McClelland, Phys. Rev. C **32**, 239 (1985).

[82] R. Abegg, D. Bandyopadhyay, J. Birchall, C. A. Davis, N. E. Davison, P. W. Green, L. G. Greeniaus, C. Lapointe, C. A. Miller, G. A. Moss, S. A. Page, W. D. Ramsay, R. R. Tkachuk, and W. T. H. van Oers, Phys. Rev. C **38**, 2173 (1988).